Cell

Intermittent fasting triggers interorgan communication to suppress hair follicle regeneration

Graphical abstract

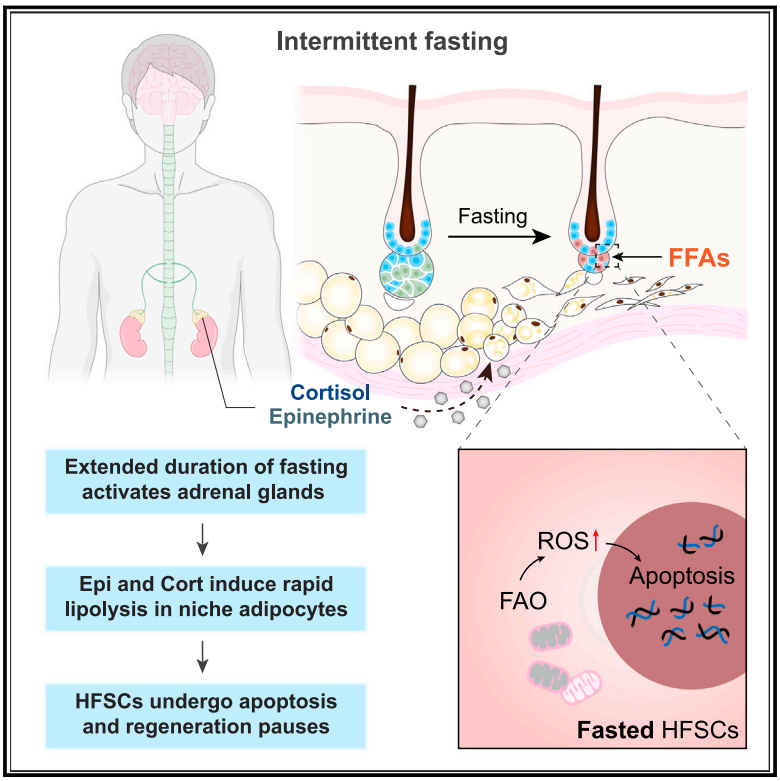

Authors

Han Chen, Chao Liu, Shiyao Cui, ..., Jufang Zhang, Ju-Sheng Zheng, Bing Zhang

Correspondence

zhangbing@westlake.edu.cn

In brief

Intermittent fasting halts hair follicle regeneration by activating communication between adrenal glands and niche adipocytes, which in turn selectively induces apoptosis of hair follicle stem cells but not epidermal stem cells in the skin.

Highlights

- Common intermittent fasting regimens inhibit hair follicle regeneration in mice
- Fasting selectively eliminates activated HFSCs, but not EpiSCs that maintain epidermis
- Activated adrenal gland-dermal adipocyte crosstalk mediates HFSC apoptosis
- Intermittent fasting inhibits human hair growth in a randomized clinical trial

Chen et al., 2025, Cell *188*, 1–18
January 9, 2025
https://doi.org/10.1016/j.cell.2024.11.004

CellPress

Cell

CellPress

Article

Intermittent fasting triggers interorgan communication to suppress hair follicle regeneration

Han Chen,[1,2,7] Chao Liu,[2,7] Shiyao Cui,[2,7] Yingqian Xia,[2,3,4] Ke Zhang,[2] Hanxiao Cheng,[5] Jingyu Peng,[2,8] Xiaoling Yu,[2] Luyang Li,[2] Hualin Yu,[1,2] Jufang Zhang,[5] Ju-Sheng Zheng,[2,6] and Bing Zhang[2,3,4,9,*]

[1]College of Life Sciences, Zhejiang University, Hangzhou, Zhejiang 310000, China
[2]School of Life Sciences, Westlake University, Hangzhou, Zhejiang 310000, China
[3]Westlake Laboratory of Life Sciences and Biomedicine, Hangzhou, Zhejiang 310000, China
[4]Research Center for Industries of the Future, Westlake University, Hangzhou, Zhejiang 310000, China
[5]Department of Plastic Surgery, Affiliated Hangzhou First People's Hospital, School of Medicine, Westlake University, Hangzhou, Zhejiang 310000, China
[6]School of Medicine, Westlake University, Hangzhou, Zhejiang 310000, China
[7]These authors contributed equally
[8]Present address: Department of Stem Cell and Regenerative Biology, Harvard University, Cambridge, MA 02138, USA
[9]Lead contact
*Correspondence: zhangbing@westlake.edu.cn
https://doi.org/10.1016/j.cell.2024.11.004

SUMMARY

Intermittent fasting has gained global popularity for its potential health benefits, although its impact on somatic stem cells and tissue biology remains elusive. Here, we report that commonly used intermittent fasting regimens inhibit hair follicle regeneration by selectively inducing apoptosis in activated hair follicle stem cells (HFSCs). This effect is independent of calorie reduction, circadian rhythm alterations, or the mTORC1 cellular nutrient-sensing mechanism. Instead, fasting activates crosstalk between adrenal glands and dermal adipocytes in the skin, triggering the rapid release of free fatty acids into the niche, which in turn disrupts the normal metabolism of HFSCs and elevates their cellular reactive oxygen species levels, causing oxidative damage and apoptosis. A randomized clinical trial (NCT05800730) indicates that intermittent fasting inhibits human hair growth. Our study uncovers an inhibitory effect of intermittent fasting on tissue regeneration and identifies interorgan communication that eliminates activated HFSCs and halts tissue regeneration during periods of unstable nutrient supply.

INTRODUCTION

Fasting has been a longstanding tradition among many religious groups for centuries. In recent years, various intermittent fasting regimens incorporating periodic fasting or time-restricted eating schedules have become increasingly popular worldwide. Growing evidence suggests that these fasting paradigms not only benefit metabolic health and weight control[1–4] but also exert profound effects on tissue health,[5–9] although the mechanisms of such impacts are not well understood. Somatic stem cells are the driving force for the maintenance and regeneration of many tissues throughout the body. Within tissues, somatic stem cells reside in a specialized microenvironment called the "niche."[10,11] Niche integrates signals from both local and systemic sources to determine the fate of stem cells and modulate regenerative processes in response to diverse physiological and environmental changes, which are critical for animals' adaptation and survival in nature.[12] However, the detailed mechanisms by which intermittent fasting affects somatic stem cells and their niches are not fully understood. Establishing these mechanisms is crucial for understanding the root cause of intermittent fasting's effects on tissue health.

Previous studies have shown that fasting improves the function and stress resistance of multiple somatic stem cell populations in the intestine, muscle, and hematopoietic system.[13–16] However, the effects of intermittent fasting on other peripheral tissues, such as the skin, have not been determined. Mechanistically, intermittent fasting leads to extended intervals between meals, changes in circadian rhythm, and reduced overall calorie intake.[6] Nevertheless, it remains unclear which of these factors primarily drives the impacts of intermittent fasting on somatic stem cells and tissue regeneration. Additionally, intermittent fasting causes considerable shifts in body physiology, but the pathways by which these systemic changes are communicated to peripheral tissues and whether specific niche components play a role in influencing stem cell fate remain largely unknown.

Please cite this article in press as: Chen et al., Intermittent fasting triggers interorgan communication to suppress hair follicle regeneration, Cell (2025), https://doi.org/10.1016/j.cell.2024.11.004

Lastly, somatic stem cells often exhibit unique metabolic signatures,[17–19] utilizing distinct metabolic programs during various stages of tissue regeneration.[20,21] However, how these inherent properties shape their unique responses to fasting is not clear.

Here, we investigated these questions in the skin. Within the skin, the hair follicles undergo cyclic phases of growth (anagen), regression (catagen), and rest (telogen) to produce new hairs, driven by the periodic activation of hair follicle stem cells (HFSCs).[22–24] During telogen, HFSCs remain quiescent in the hair follicle's bulge and hair germ regions.[25–27] They become transiently active upon anagen entry, initiating hair follicle regeneration and performing self-renewal[12,28] (Figure S1A). Additionally, diverse cell types in the skin organize into a complex niche surrounding the HFSCs,[29] enabling the modulation of their regenerative activities in response to external stimuli or physiological changes.[30,31] Prior clinical observations suggest that patients on very low-calorie diets for rapid weight loss may experience hair loss.[32,33] However, the effects of modern intermittent fasting regimens on hair follicle regeneration and hair growth remain unclear. The well-defined behaviors of HFSCs and the visible nature of the hair make the hair follicle an ideal system for studying how various intermittent fasting regimens impact somatic stem cells and tissue biology.

RESULTS

Commonly used intermittent fasting regimens inhibit hair follicle regeneration

To examine the effects of intermittent fasting on hair follicle regeneration, we adopted two commonly used intermittent fasting regimens: 16/8 time-restricted feeding (TRF), where daily food consumption is limited to an 8-h window followed by a 16-h fasting period, and alternate-day fasting (ADF), which involves alternating between a 24-h fasting period and a 24-h unrestricted eating period[6] (Figure 1A). We applied these paradigms on adult C57BL/6 mice starting from postnatal day (P) 60, when the hair follicles on their back skin were at the extended 2nd telogen phase, before anagen entry (Figure S1A). The mice were shaved before treatments, and their hair regrowth was monitored over a 96-day treatment period until P156 (Figure 1B). Animals under regular *ad libitum* (AL) feeding entered anagen around P80 and had most of their back hair regrown by P100. By contrast, animals subjected to the TRF or ADF paradigms exhibited significantly impaired hair follicle regeneration, with only partial hair regrowth observed by P156 (Figures 1B and 1C). Hematoxylin and eosin (H&E) staining revealed that hair follicles from the treated groups were stuck in an extended telogen/early anagen phase, resulting in a lack of new hair shaft production (Figure 1D). This inhibitory effect can be observed in both male and female mice, as well as in mice treated from P24, a stage when their back skin hair follicles were in the 1st telogen phase (Figures S1A–S1E). We monitored the animals' food intakes and metabolic status using metabolic cages and confirmed that the fasting paradigms were effectively performed (Figures 1E and S1F). In addition, consistent with previous reports,[34,35] mice subjected to intermittent fasting exhibited enhanced glucose tolerance, an indicator of improved metabolic health (Figure S1G). Collectively, these findings indicate that while commonly used intermittent fasting regimens offer metabolic benefits, they exhibit substantial inhibitory effects on hair follicle regeneration.

Intermittent fasting selectively induces apoptosis in activated HFSCs

Next, we aimed to analyze how intermittent fasting impacts the fates of HFSCs (Figure 2A). HFSCs in the bulge exhibit expression of high CD34 and low P-cadherin (CD34^{high}/Pcad^{low}), while HFSCs in the hair germ are CD34^{low}/Pcad^{high}.[36] Upon entering anagen, HFSCs in the hair germ are activated first, followed by those in the bulge. These activated HFSCs further develop into a highly proliferative transit-amplifying progenitor population (HF-TACs) with elevated ephrin-B1 expression, driving hair follicle growth (Figure 2A). Failure to activate quiescent HFSCs is a common cause of many hair follicle regeneration defects.[31,37] To test whether intermittent fasting inhibits HFSC activation, we applied ADF to mice starting from P24, when their hair follicles were in telogen and HFSCs in the quiescent state, and examined HFSCs daily for activation defects. 5-ethynyl-2′-deoxyuridine (EdU, a thymidine analog that incorporates into the DNA of dividing cells) was injected to label proliferative HFSCs. Mice under AL could activate HFSCs and enter anagen by P26, as evidenced by the EdU+ HFSCs within their hair follicles (Figures 2B, AL, green arrowhead and S2A). Similarly, mice subjected to ADF could also activate a comparable number of HFSCs by P26 (Figures 2B, ADF, yellow arrowhead and S2A). However, following the 24-h fasting period, the number of EdU+ HFSCs within their hair follicles decreased dramatically, while many apoptotic signals appeared, as evidenced by the staining of active caspase-3 (Figures 2B, ADF, red arrowhead and S2B). During the subsequent feeding period, more HFSCs were activated, only to be eliminated again by fasting. As a result, HFSCs were activated and eliminated repetitively during intermittent fasting, leading to insufficient production of HF-TACs and inhibited hair follicle growth (Figures 2B and S2C). Whole-mount staining confirmed the extensive HFSC apoptosis after 24 h of fasting (Figure 2C). Similarly, apoptotic HFSCs can be found in mice under TRF as well as in mice with intermittent fasting starting from the 2nd telogen phase (Figures S2D and S2E).

To determine whether activated HFSCs are selectively eliminated by fasting, we labeled proliferative HFSCs by injecting EdU intraperitoneally every 6 h during a 24-h feeding period in mice subjected to ADF and then traced the fate of these cells after the 24-h fasting period (Figure 2D). Most apoptotic HFSCs were positive for EdU, indicating that they were previously activated before undergoing apoptosis (Figure 2D). Flow cytometry analysis showed that approximately 25% of HFSCs were activated during the feeding period in ADF, and approximately 90% of them were eliminated after fasting (Figure 2E), leading to a significant decrease in total HFSC number after multiple rounds of fasting in ADF (Figure 2F). By contrast, quiescent HFSCs within either 1st or 2nd telogen hair follicles did not show any apoptotic signal after 24-h fasting (Figures S2F and S2G), suggesting that only activated HFSCs are affected by fasting. To further confirm this, we artificially activated quiescent HFSCs in the 2nd telogen hair follicles by hair plucking,[38] and subsequently implemented ADF (Figure 2G). Hair plucking

Please cite this article in press as: Chen et al., Intermittent fasting triggers interorgan communication to suppress hair follicle regeneration, Cell (2025), https://doi.org/10.1016/j.cell.2024.11.004

CellPress

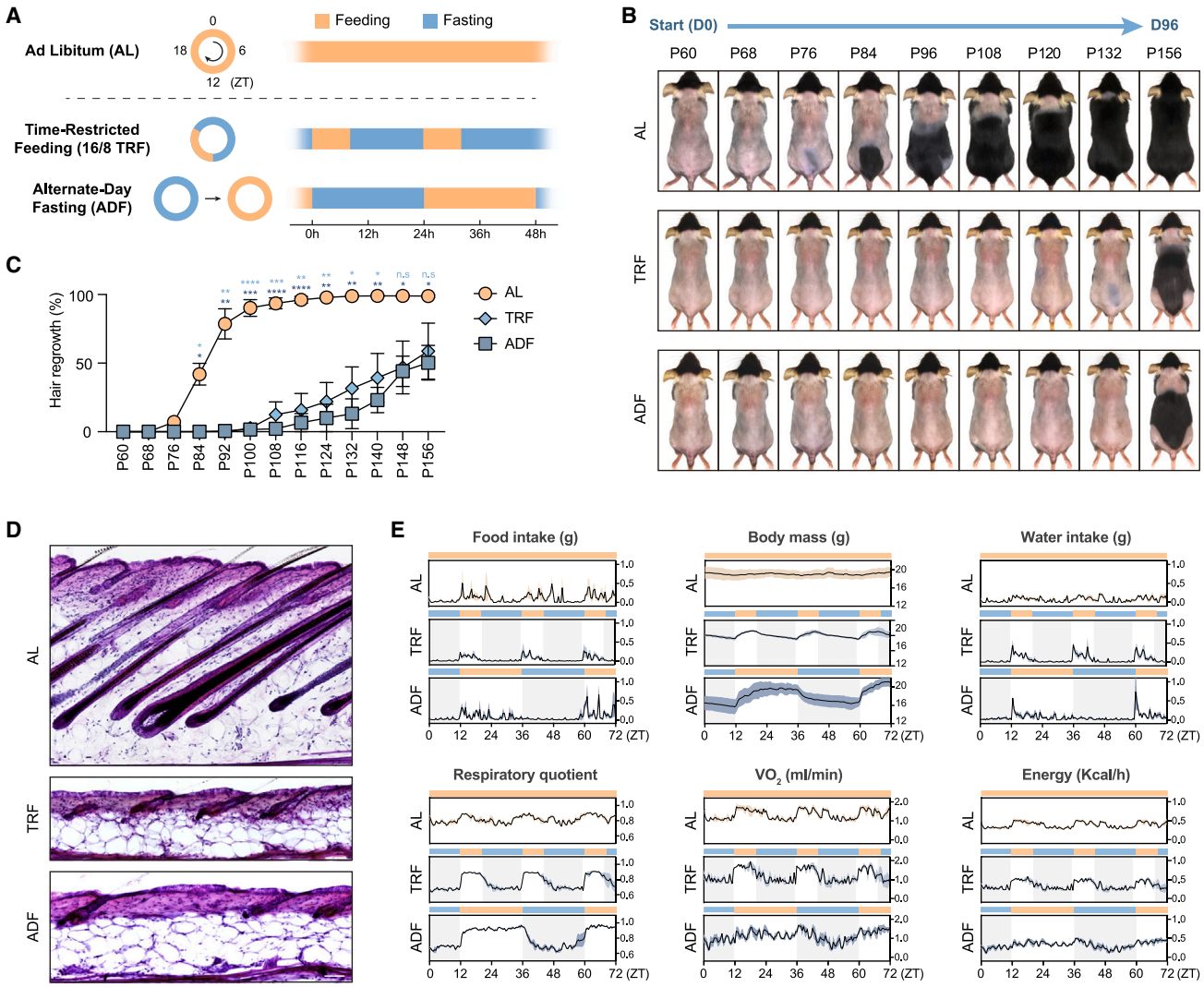

Figure 1. Intermittent fasting inhibits hair follicle regeneration

(A) Schematic of dietary intervention paradigms, including AL, 16/8 TRF, and ADF. Feeding starts from zeitgeber time (ZT) 12 after lights off.

(B) Progression of hair regrowth in female mice subjected to AL, 16/8 TRF, and ADF between P60 and P156. Mice were shaved before treatments (n = 8–10).

(C) Quantification of the hair regrowth in mice in (B) (n = 5, two-way ANOVA).

(D) H&E staining of skin. Scale bar, 100 μm.

(E) Metabolic cage data of mice under AL, TRF, and ADF over a 72-h period starting from ZT0. Fasting periods are shadowed by gray. Parameters measured: food intake (gram), body mass (gram), water intake (gram), respiratory quotient (VCO_2/VO_2), the volume of oxygen consumed VO_2 (mL/min), and energy expenditure (kcal/h, n = 3). Data are presented as mean ± SEM. *p <0.05, **p < 0.01, ***p < 0.001, ****p < 0.0001, n.s., not significant.

See also Figure S1.

activates a greater number of HFSCs compared with natural anagen entry (Figure S2H). With the increased number of active HFSCs, more apoptotic HFSCs were observed after fasting (Figure 2G). Consequently, the number of HFSCs decreased dramatically in fasted mice compared with mice under AL (Figure S2I), and a significant delay in hair follicle regeneration and hair regrowth was observed (Figure 2H). Fasting-induced apoptotic signals were also observed in anagen hair follicles in the tail skin but not in telogen hair follicles in the ear skin (Figures S2J and S2K). Additionally, apoptosis was observed in melanocyte stem cells (McSCs) that share the same niche and are activated together with HFSCs, but not in other skin cell types, including epidermal stem cells (EpiSCs), keratin 6+ inner bulge cells, dermal fibroblasts, or immune cells (Figures S2L–S2O). After a significant delay, pigmented hairs can regrow in some areas of the back skin (Figures 1B and S1B), likely due to the accumulation of the remaining activated HFSCs and McSCs after fasting (Figures S2C and S2L), which continue to differentiate and drive hair follicle growth and pigment production (Figure S2P).

To assess the potential long-term effects of intermittent fasting on HFSCs, we applied intermittent fasting paradigm TRF on mice

Please cite this article in press as: Chen et al., Intermittent fasting triggers interorgan communication to suppress hair follicle regeneration, Cell (2025), https://doi.org/10.1016/j.cell.2024.11.004

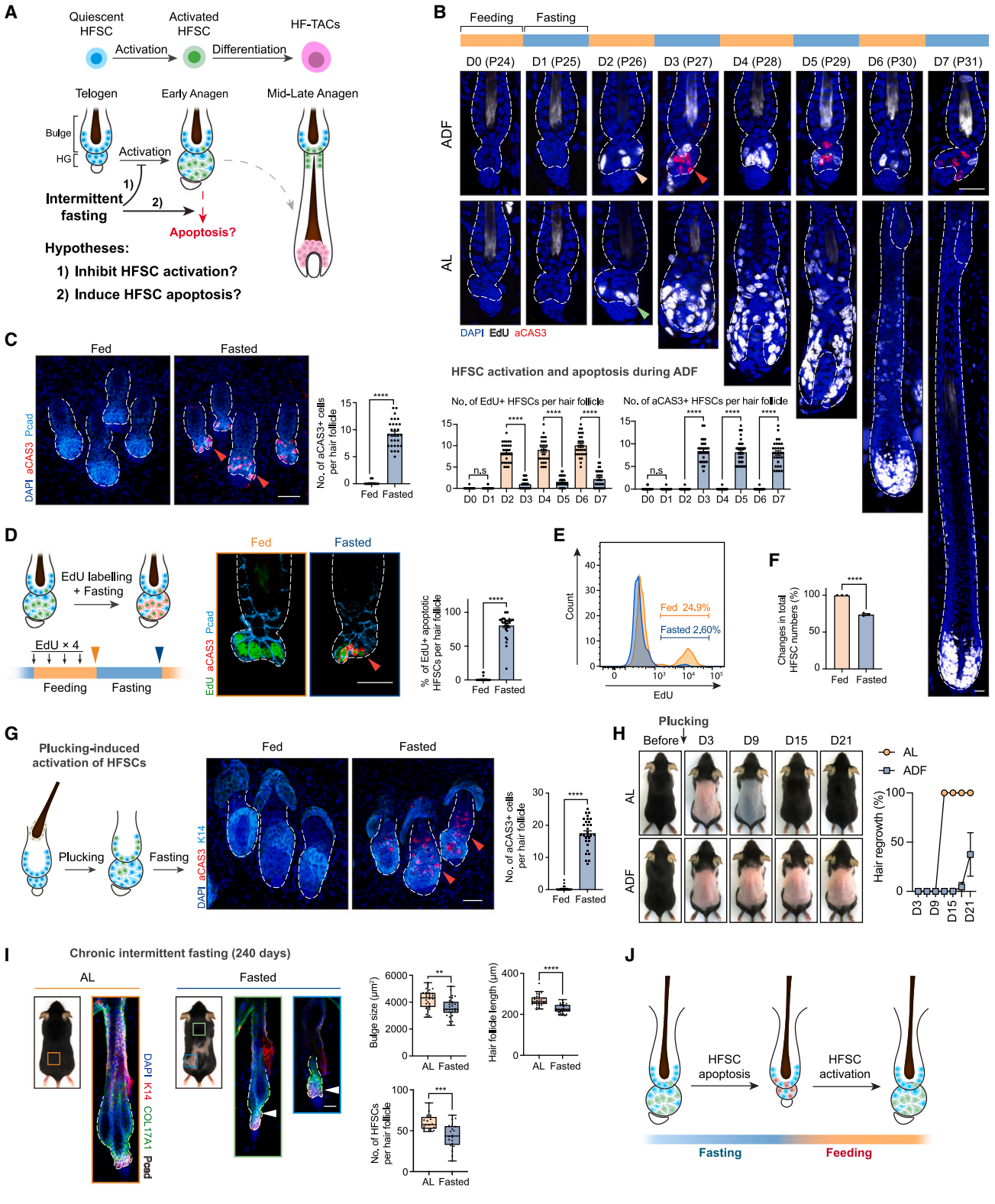

(legend on next page)

Please cite this article in press as: Chen et al., Intermittent fasting triggers interorgan communication to suppress hair follicle regeneration, Cell (2025), https://doi.org/10.1016/j.cell.2024.11.004

for 8 months. Chronic application of intermittent fasting resulted in baldness in some regions of their back skin (Figure 2I). Upon examination of hair follicles, we observed a significant reduction in HFSC number, hair follicle length, and HFSC compartment size (Figure 2I), indicative of hair follicle degeneration driven by stem cell loss.[39] Collectively, these data suggest that under intermittent fasting, HFSCs undergo repetitive cycles of activation and apoptosis (Figure 2J). When implemented for a short-term, intermittent fasting disrupts the normal progression of the hair follicle regeneration program into later stages, resulting in delayed hair follicle regeneration. When applied chronically, they cause HFSC loss and hair follicle degeneration.

Extended duration of fasting drives stem cell death

Intermittent fasting is generally believed to achieve its effects through the reduction of overall calorie intake and modification of eating patterns, often involving cycles of extended fasting (Figure 3A). To determine whether the regeneration defect was due to reduced overall calorie intake, we closely examined the daily food consumption of our experimental mice. Contrary to our expectations, mice subjected to either TRF or ADF did not exhibit a significant decrease in average daily calorie intake compared with those under AL (Figure 3B). Further analysis revealed that these mice quickly adapted to the feeding schedules by adjusting eating behaviors to consume more food within the designated feeding windows (Figure 3C). Therefore, the apoptosis of HFSCs cannot be attributed to a reduction in total calorie intake.

Extended duration of fasting is another key component embedded within various intermittent fasting regimens. Mice subjected to 16/8 TRF experience 16 h of fasting daily, while mice subjected to ADF experience 24 h of fasting every other day (Figures 1A and 1E). To determine if the apoptosis of HFSCs correlates with the length of fasting duration, we subjected mice to varying lengths of fasting and examined the occurrence of HFSC apoptosis (Figure 3D). After 8 h of fasting, the hair follicles had minimal apoptotic signals. However, as the fasting duration increased to 16 h, many apoptotic HFSCs appeared. The number of apoptotic HFSCs continued to rise with longer fasting durations and disappeared after refeeding (Figure 3D). To further confirm that extended fasting duration mediated the inhibitory effect of intermittent fasting on hair follicle regeneration, we modified the typical 16/8 TRF paradigm by extending the daily feeding window from 8 to 12 h (Figures 3E and 3F). Despite no significant increase in food consumption, mice with a longer feeding window (thus shorter daily fasting time) exhibited nearly normal hair regrowth (Figures 3G–3I). By contrast, when we implemented more stringent TRF paradigms with a daily feeding window reduced from 8 to 5 or 3 h, without significant reduction in food intake, mice with longer daily fasting time exhibited more pronounced delays in hair regrowth (Figures 3E–3I). In addition, fasting during either the day or the night resulted in similar delays in hair follicle regeneration, indicating that the defects cannot be attributed to changes in circadian rhythms (Figures S3A–S3C). Together, these findings suggest that the apoptosis of HFSCs and hair follicle regeneration defects are primarily caused by extended durations of fasting embedded within various intermittent fasting regimens, rather than reduced overall calorie intake or circadian rhythm changes. As the fasting period lengthens, the severity of the defects worsens. Because the ADF paradigm induces severe HFSC apoptosis and hair follicle regeneration defects, we focus on using ADF for most of the remaining mechanistic studies.

Fasting-induced lipolysis in niche adipocytes drives HFSC apoptosis

Next, we aimed to identify the mechanism by which extended fasting impacts HFSCs. Fasting induces a temporary fall in systemic nutrient levels, which could be directly sensed by HFSCs' cellular nutrient-sensing mechanisms, eventually leading to apoptosis[40] (Figure 4A). To test this possibility, we first measured the blood glucose levels throughout the 24-h fasting and 24-h refeeding cycle in mice under ADF (Figures 4B and S4A). Following fasting, blood glucose levels drop significantly, indicating a temporal reduction in systemic nutrient levels (Figure 4B). As the mammalian target of rapamycin (mTOR) signaling pathway serves as the primary cellular nutrient-sensing mechanism in HFSCs,[41] we generated *K15*^{CrePGR}*; Tsc2*$^{fl/fl}$ mice to knockout tuberous sclerosis complex 2 (*Tsc2*), the negative regulator of the mammalian target of rapamycin complex 1

Figure 2. Intermittent fasting induces apoptosis in activated HFSCs

(A) Possible mechanisms of inhibited hair follicle (HF) regeneration.

(B) Activation and apoptosis of HFSCs in mice subjected to AL and ADF starting from P24. Antibodies stained: active caspase-3 (aCAS3, $n = 30$ HFs from 5 mice, one-way ANOVA).

(C) Whole-mount staining of HFs from mice subjected to 24-h fasting at P27. Antibodies stained: P-cadherin (Pcad, outlining the HFSC compartment), aCAS3 ($n = 30$ HFs from 3 mice, two-tailed unpaired t test).

(D) Tracing the fate of activated HFSCs upon intermittent fasting ($n = 30$ HFs from 5 mice, two-tailed unpaired t test).

(E and F) (E) Flow cytometry analysis showing the proportion of EdU+ HFSCs and (F) total number of HFSCs decrease after a 24-h fasting period in ADF ($n = 3$, two-tailed unpaired t test).

(G) Fasting induces apoptosis of HFSCs that were artificially activated by hair plucking. Antibodies stained: keratin 14 (K14, outlining the HF), aCAS3 ($n = 30$ HFs from 3 mice, two-tailed unpaired t test).

(H) Delayed hair regrowth after hair plucking upon ADF ($n = 3$).

(I) Left: changes in HF morphology after 8 months of intermittent fasting. Antibodies stained: Pcad, K14, and collagen 17A1 (a marker for HFSCs). White arrowheads indicate degenerated HFs. Right: quantification of HFSC compartment size, HF length, and HFSC numbers ($n = 30$ HFs from 3 mice, two-tailed unpaired t test).

(J) Model summarizing the cyclic activation and apoptosis of HFSCs during intermittent fasting. Scale bars, 30 μm. In the bar graph, data are presented as mean ± SEM. In the box plot, data are presented as the interquartile range and median. $^{**}p < 0.01$, $^{***}p < 0.001$, $^{****}p < 0.0001$, n.s., not significant.

See also Figure S2.

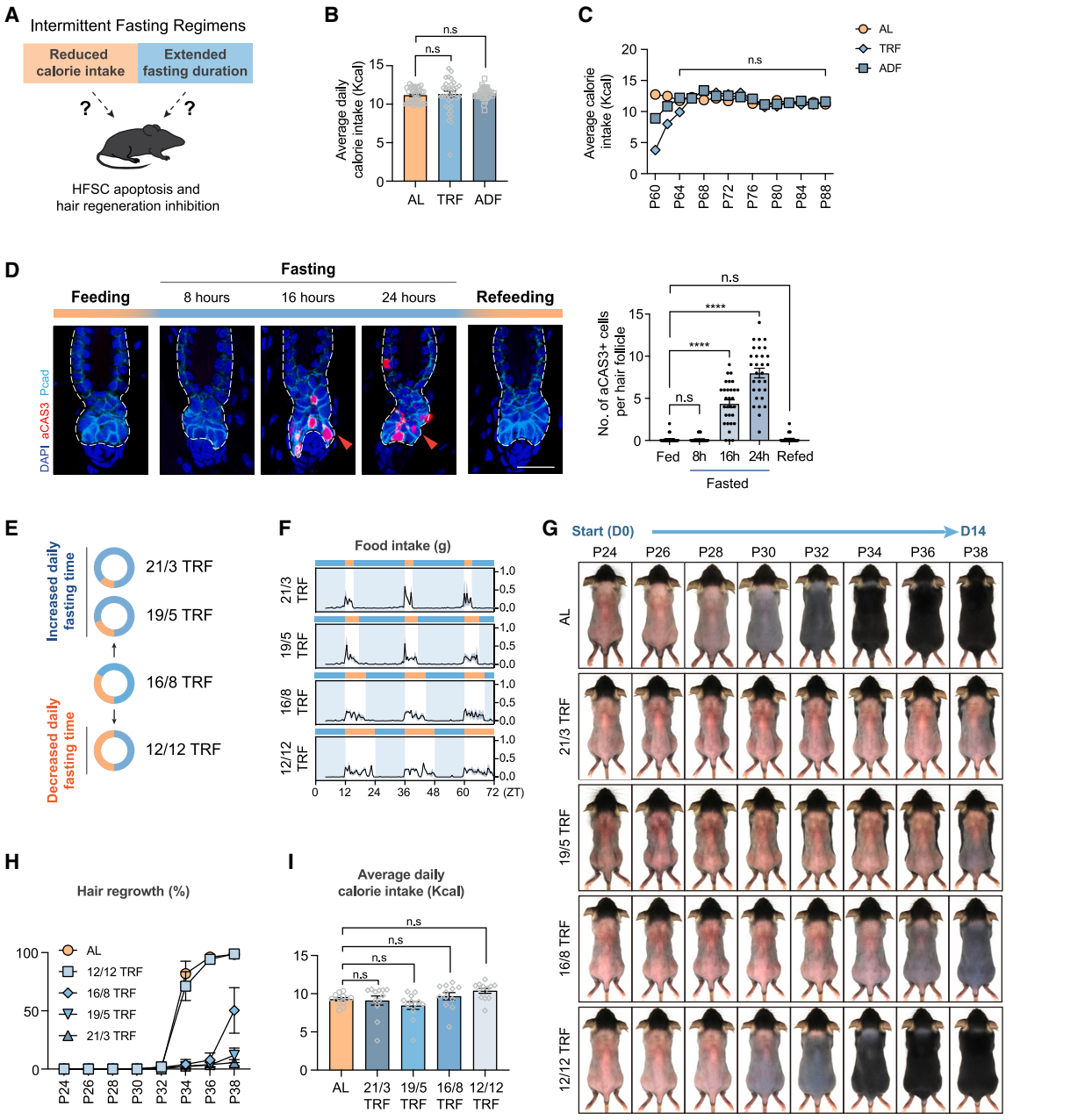

Figure 3. Extended duration of fasting induces HFSC death and inhibits hair follicle regeneration

(A) Possible factors that cause HFSC apoptosis and HF regeneration inhibition.

(B) Average daily calorie intake of female mice under AL, TRF, and ADF between P60 to P130 (n = 35 days of calorie intake record from 5 mice, one-way ANOVA).

(C) Daily calorie intake records from P60 to P88 (n = 5).

(D) Time course of HFSC apoptosis along the 24-h fasting and 24-h refeeding periods. Red arrowheads mark the apoptotic HFSCs. (n = 30 HFs from 5 mice, one-way ANOVA.)

(E) Manipulating the duration of fasting in TRF.

(F) Metabolic cage monitors the food intake of mice under different TRFs (n = 3).

(G and H) Hair regrowth in mice under different TRFs (n = 3–5).

(I) Average daily calorie intake (n = 12 days of caloric intake record from 5 mice, one-way ANOVA). Scale bar, 30 μm. Data are presented as mean ± SEM. ****p < 0.0001, n.s., not significant.

See also Figure S3.

Please cite this article in press as: Chen et al., Intermittent fasting triggers interorgan communication to suppress hair follicle regeneration, Cell (2025), https://doi.org/10.1016/j.cell.2024.11.004

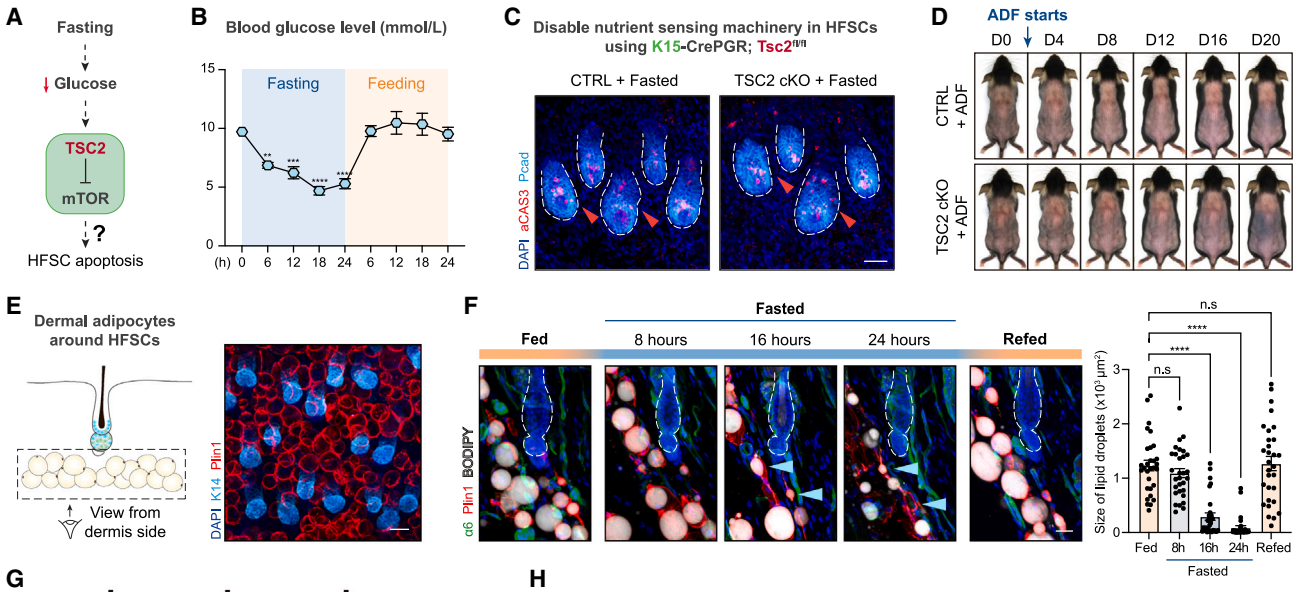

(legend on next page)

Please cite this article in press as: Chen et al., Intermittent fasting triggers interorgan communication to suppress hair follicle regeneration, Cell (2025), https://doi.org/10.1016/j.cell.2024.11.004

(mTORC1) signaling pathway, specifically from HFSCs (Figure S4B). Without TSC2, the mTORC1 signaling pathway becomes constitutively active, losing its functional nutrient-sensing ability.[42] Despite this, HFSCs in the *Tsc2* knockout mice still underwent apoptosis following fasting, resulting in delayed hair regrowth, while HFSC activation and hair growth remained unaffected under AL (Figures 4C, 4D, and S4C). Hence, fasting-induced apoptosis in HFSCs is not dependent on the classical mTORC1 cellular nutrient-sensing mechanism.

Extended duration of fasting also triggers a range of evolutionarily conserved adaptative responses to initiate fitness behaviors and mobilize stored fats from adipose tissues.[43–46] Within the skin, adipocytes in the dermis are crucial components of the HFSC niche[47,48] (Figure 4E). Therefore, we asked if systemic changes induced by fasting could transmit into the skin and influence HFSCs through niche adipocytes. Indeed, after 24 h of fasting, dermal adipocytes underwent extensive lipolysis to break down stored triglycerides, releasing substantial amounts of free fatty acids (FFAs) into the niche (Figures S4D–S4G). As a result, the local FFA concentration in the skin far exceeds that found in circulation (Figure S4G). To test whether the lipolysis in dermal adipocytes correlates with HFSC death, we monitored their lipolysis process across the 24-h fasting period in ADF. Notably, prominent lipolysis in dermal adipocytes can be observed after 16 h of fasting (Figure 4F, blue arrowheads), coinciding with the appearance of apoptotic HFSCs in the hair follicle (Figure 3D). Once the mice were fed, the lipolysis of dermal adipocytes ceased promptly, and the apoptosis of HFSCs also subsided (Figures 3D and 4F). Together, these data imply a strong link between dermal adipocyte lipolysis and HFSC apoptosis during fasting.

To determine whether fasting-induced lipolysis in dermal adipocytes drives HFSC death, we generated *AdipoQ*^{CreER}*; Atgl*$^{fl/fl}$ mice to knockout adipose triglyceride lipase (*Atgl*),[49] a critical lipolytic enzyme, specifically from dermal adipocytes (Figures 4G and S4H). Without ATGL, dermal adipocytes became resistant to fasting-induced lipolysis (Figure 4H, lower). Simultaneously, a significant reduction in HFSC apoptosis was observed upon fasting (Figure 4H, upper). To determine if the oxidation of these excessive FFAs by HFSCs induces apoptosis, we generated *Lhx2*^{CreER}*; Cpt1a*$^{fl/fl}$ mice to knockout carnitine palmitoyltransferase 1A (*Cpt1a*), a rate-limiting enzyme responsible for transporting FFAs into the mitochondrial matrix for beta-oxidation,[14] specifically from HFSCs (Figures 4G and S4I). Although with extensive lipolysis in dermal adipocytes, genetic blocking of fatty acid oxidation (FAO) in HFSCs significantly reduced their apoptosis upon fasting (Figure 4I), and the inhibited hair follicle regeneration in mice subjected to ADF was also alleviated (Figure 4J). The surviving HFSCs with *Cpt1a* knockout exhibited reduced proliferation during fasting compared with AL (Figure S4J). Treatment with the glutaminase inhibitor CB-839 induced significant apoptosis in these HFSCs upon fasting but not under AL (Figures 4K and S4K). These findings suggest that HFSCs with *Cpt1a* knockout reduce proliferation during fasting and likely depend on glutamine metabolism as an alternative energy source to maintain survival. Under AL, HFSC activation, lipolysis in dermal adipocytes, and hair cycle progression remain largely unaffected in these genetic knockout models (Figures S4L–S4Q). Thus, excessive FFAs released from dermal adipocytes and their oxidation in HFSCs drive the apoptosis of HFSCs upon fasting, and this pathway remains inactive under AL feeding conditions.

To further determine if elevated levels of FFAs in the niche are sufficient to drive HFSC apoptosis without fasting, we purified dermal adipocytes from the skin and analyzed the composition of FFAs within their triglycerides using gas chromatography-mass spectrometry (GC-MS). The most abundant FFA species are palmitic acid (16:0), oleic acid (18:1, *cis*-9), and linoleic acid (18:2, *cis*-9,12, Figure 4L). Intradermal injection of these FFAs into a small region of the skin induced apoptosis in HFSCs without fasting but not in EpiSCs (Figures 4M, S4R, and S4S). Collectively, our data demonstrate that fasting-induced lipolysis in dermal adipocytes and FAO in HFSCs are pivotal processes driving HFSC apoptosis during intermittent fasting.

Fasting activates adrenal glands to halt tissue regeneration

To investigate how fasting signals are transmitted into the skin and induce lipolysis in dermal adipocytes, we started by examining the role of sympathetic nerves, which serve as a crucial mediator of the body's response to low energy levels[50] (Figure 5A). Inside the skin, postganglionic sympathetic nerves are

Figure 4. Fasting-induced lipolysis in niche adipocytes drives HFSC apoptosis

(A) Possible mechanisms of fasting-induced HFSC apoptosis through the mTORC1 pathway.
(B) Blood glucose changes during the 24-h fasting and 24-h refeeding periods. (n = 6, one-way ANOVA.)
(C) Whole-mount staining of HFs from *K15*^{CrePGR}*; Tsc2*$^{fl/fl}$ mice and littermate controls for aCAS3 and Pcad under ADF (n = 5).
(D) Delayed hair regrowth in *K15*^{CrePGR}*; Tsc2*$^{fl/fl}$ mice and littermate controls under ADF (n = 3).
(E) Whole-mount staining of dermal adipocytes (Plin1, marks the surface of lipid droplets) and HFs (K14).
(F) Time course of dermal adipocyte lipolysis along the 24-h fasting and 24-h refeeding periods. α6 outlines the HF, and BODIPY marks lipid droplets (n = 30 lipid droplets from 3 mice, one-way ANOVA).
(G) Possible mechanisms of fasting-induced HFSC apoptosis. TAG, triglyceride; DAG, diglyceride; MAG, monoglyceride.
(H and I) (H) Lipolysis of dermal adipocytes (bottom) and apoptosis of HFSCs (top) in *AdipoQ*^{CreER}*; Atgl*$^{fl/fl}$ (ATGL cKO) mice or (I) *Lhx2*^{CreER}*; Cpt1a*$^{fl/fl}$ (CPT1A cKO) mice after 24-h fasting (n = 30 HFs from 6 mice, two-tailed unpaired t test).
(J) Hair regrowth in *Lhx2*^{CreER}*; Cpt1a*$^{fl/fl}$ mice and littermate controls under ADF (n = 3).
(K) Apoptosis of HFSCs in CPT1A cKO mice treated with CB-839 after 24-h fasting (n = 30 HFs, two-tailed unpaired t test).
(L) GC-MS analysis of FFA composition in dermal adipocytes (n = 4).
(M) Apoptosis of HFSCs upon FFAs intradermal injection on AL mice. (n = 30 HFs from 3 mice, one-way ANOVA.) Scale bars, 30 μm. Data are presented as mean ± SEM. ****p < 0.0001, n.s., not significant.
See also Figure S4.

Please cite this article in press as: Chen et al., Intermittent fasting triggers interorgan communication to suppress hair follicle regeneration, Cell (2025), https://doi.org/10.1016/j.cell.2024.11.004

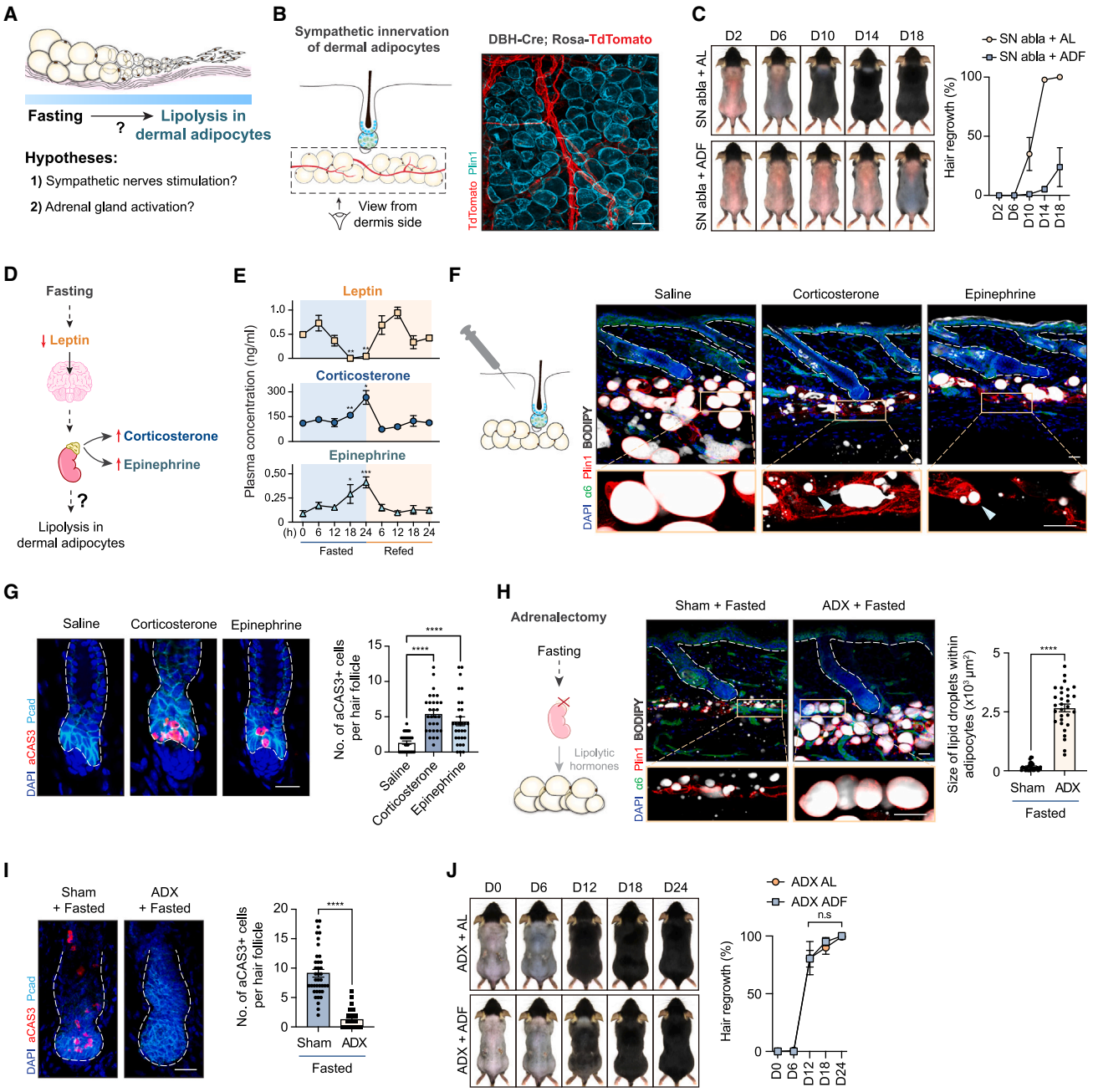

Figure 5. Fasting activates adrenal glands to induce lipolysis in niche adipocytes and apoptosis in HFSCs

(A) Possible mechanisms of fasting-induced lipolysis in dermal adipocytes.

(B) Sympathetic innervation of dermal adipocytes in mice back skin. Whole-mount staining for Plin1 in *DBH-Cre;Rosa-TdTomato* mice, TdTomato marks sympathetic nerves.

(C) Inhibited hair regrowth in sympathetic nerve ablated (SN abla) mice upon ADF ($n = 5$).

(D) Schematic of fasting-induced adrenal gland activation.

(E) ELISA measurement of plasma leptin, corticosterone, and epinephrine levels during the 24-h fasting and 24-h refeeding periods. ($n = 5$, one-way ANOVA.)

(F and G) (F) Intradermal injection of corticosterone or epinephrine causes lipolysis of dermal adipocytes and (G) apoptosis of HFSCs. ($n = 30$ HFs from 3 mice, one-way ANOVA.)

(H) Fasting-induced lipolysis in dermal adipocytes was blocked in adrenalectomized (ADX) mice. ($n = 30$ lipid droplets from 3 mice, one-way ANOVA.)

(I) Fasting-induced apoptosis of HFSCs was blocked in ADX mice. ($n = 30$ HFs from 3 mice, one-way ANOVA.)

(J) Hair regrowth in ADX mice became insensitive to intermittent fasting ($n = 6$, two-way ANOVA). Scale bars, 30 μm. Data are presented as mean ± SEM. $^{*}p < 0.05$, $^{**}p < 0.01$, $^{***}p < 0.001$, $^{****}p < 0.0001$, n.s., not significant.

See also Figure S5.

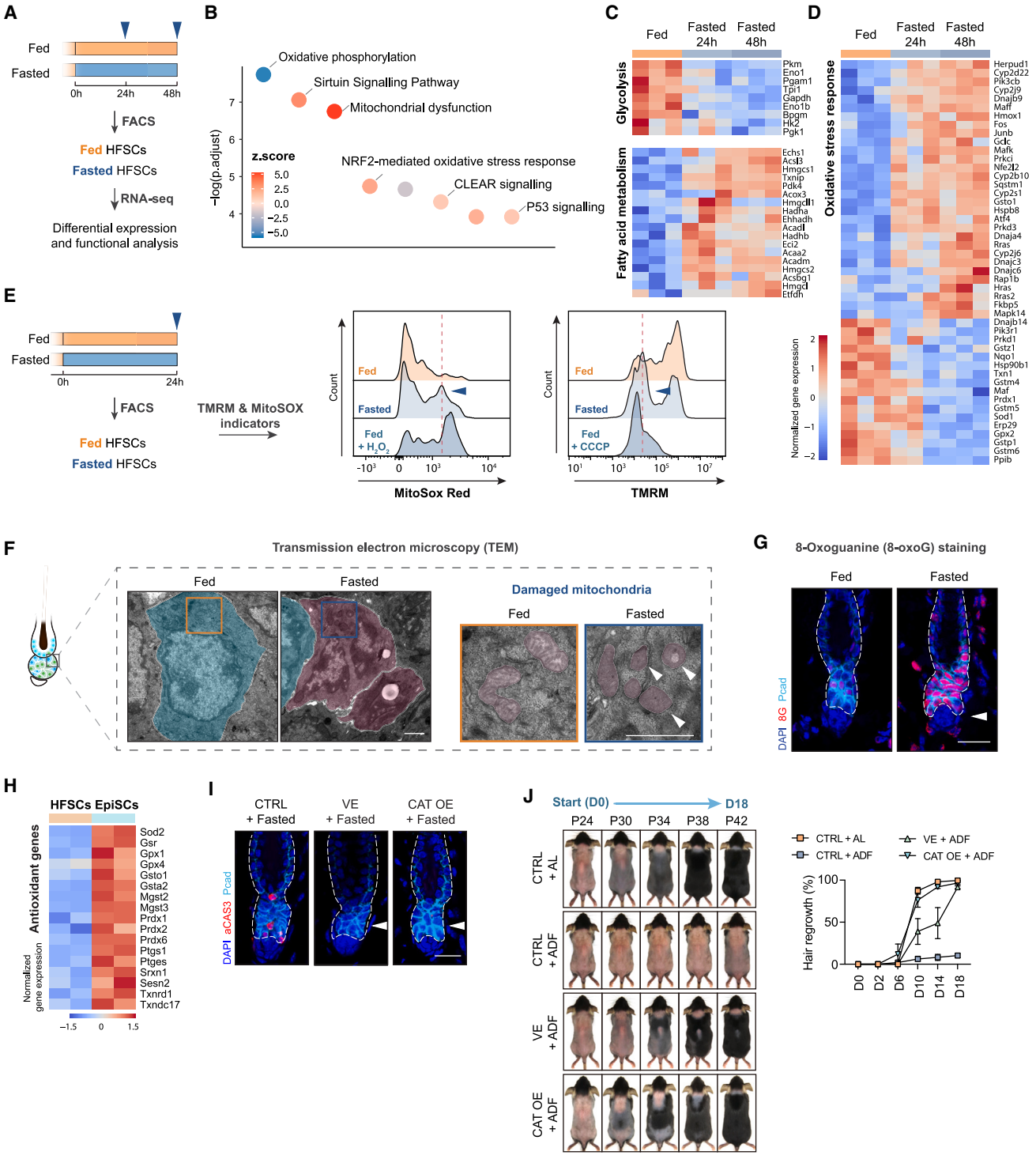

Figure 6. Elevated ROS in HFSCs leads to apoptosis, and enhancing antioxidant capability prevents HFSC apoptosis upon fasting

(A) RNA-seq workflow.

(B) IPA of differentially expressed genes (48 h fasting).

(C and D) (C) Heatmaps of signature gene expression related to glycolysis, fatty acid metabolism, and (D) oxidative stress response.

(E) Measurement of mitochondrial ROS (mROS) by MitoSox red and mitochondrial membrane potential by TMRM in HFSCs from mice upon 24-h fasting ($n = 3$). Positive controls: 500 μM H_2O_2 (for MitoSox), carbonyl cyanide m-chlorophenylhydrazone (CCCP, an oxidative phosphorylation uncoupler, for TMRM).

(legend continued on next page)

close to dermal adipocytes (Figure 5B). Upon fasting, sympathetic nerves are mildly activated, as shown by the elevated levels of FOS (a reporter for neuronal activity[51]) in the cell bodies of the sympathetic neurons (Figure S5A). To test whether sympathetic signals drive lipolysis in dermal adipocytes upon fasting, we used 6-hydroxydopamine (6-OHDA), a selective neurotoxin that targets adrenergic nerves, to remove sympathetic nerves in the skin[52] (Figure S5B). Without sympathetic innervation, dermal adipocyte lipolysis and HFSC apoptosis still exist upon fasting (Figures S5C and S5D), and the delayed hair regrowth in mice subjected to ADF was not restored (Figure 5C). Thus, sympathetic innervations do not play a significant role here.

Another possibility is the adrenal glands (Figure 5A). Adrenal glands play a central role in regulating the body's physiological adaptations to fasting.[44,53,54] Upon fasting, the fall in systemic leptin levels stimulates neurons in the hypothalamus, initiating a hormonal cascade through the hypothalamic-pituitary-adrenal (HPA) axis to prompt the release of hormones, primarily cortisol and epinephrine, from adrenal glands into the bloodstream[55–57] (Figure 5D). Both cortisol and epinephrine harbor potent lipolytic functions, and analysis of data from a previous study[58] demonstrated the expression of the β3-adrenergic receptor (ADRB3, a receptor for epinephrine) and glucocorticoid receptor (GR, a receptor for corticosterone, the mouse equivalent of cortisol) in dermal adipocytes (Figure S5E). Thus, we hypothesized that the activation of adrenal glands upon fasting induces lipolysis in dermal adipocytes, thus mediating the effects of intermittent fasting on HFSCs and hair follicle regeneration. To test this, we first monitored the activity of the adrenal glands throughout the 24-h fasting and 24-h refeeding cycle in mice under ADF by measuring the levels of leptin, epinephrine, and corticosterone in the blood every 6 h (Figure 5E). During the initial 12 h of fasting, hormone levels remained relatively stable. However, beyond this point, leptin levels significantly declined, while epinephrine and corticosterone levels increased simultaneously, indicating adrenal gland activation (Figure 5E). This was concurrent with prominent lipolysis in dermal adipocytes and the presence of apoptotic HFSCs (Figures 3D and 4F). Upon refeeding, these responses promptly ceased. These data imply a strong correlation between adrenal gland activation, dermal adipocyte lipolysis, and HFSC apoptosis during fasting.

To assess whether released corticosterone and epinephrine induce lipolysis in dermal adipocytes, we established a skin explant culture system using a low-glucose medium to mimic fasting conditions. Dose-response analyses demonstrated that physiological concentrations of these hormones under fasting can induce significant lipolysis in dermal adipocytes (Figures S5F and S5G). Moreover, intradermal injection of higher concentrations of corticosterone or epinephrine into the skin resulted in extensive lipolysis in dermal adipocytes together with apoptosis in HFSCs without fasting (Figures 5F and 5G). Notably, injecting equivalent concentrations of corticosterone or epinephrine did not induce apoptosis in HFSCs in *AdipoQ^{CreER}; Atgl$^{fl/fl}$* or *Lhx2^{CreER}; Cpt1a$^{fl/fl}$* mice (Figures S5H–S5K), suggesting that the observed apoptosis in HFSCs is due to lipolysis induced by increased levels of corticosterone or epinephrine rather than non-specific toxicity of these hormones. Furthermore, when we generated *AdipoQ^{CreER}; GR$^{fl/fl}$* mice to knockout GR specifically from dermal adipocytes (Figure S5L) or employed the beta-adrenergic antagonist propranolol to block ADRB3 signaling, the fasting-induced lipolysis in dermal adipocytes and the apoptosis in HFSCs are both significantly reduced (Figures S5M and S5N). These data suggest that both hormones play a role here. To further confirm this, we performed complete adrenalectomy surgery on mice to remove both adrenal glands (Figure 5H). Then, we subjected these mice to ADF together with sham controls. Strikingly, without adrenal glands, both fasting-induced lipolysis in dermal adipocytes and the apoptosis of HFSCs were rescued, and the hair follicle regeneration and hair regrowth also became insensitive to intermittent fasting (Figures 5H–5J). The sham control mice still showed inhibited hair regrowth upon intermittent fasting (Figure S5O). Under AL conditions, neither lipolysis in dermal adipocytes nor apoptosis in HFSCs was observed during the early anagen stage in either group (Figures S5P and S5Q). Taken together, our findings indicate that extended fasting activates the adrenal glands to release lipolytic hormones, which signal through adipocytes in the niche to eliminate activated HFSCs and inhibit hair follicle regeneration.

Fasting induces elevated ROS in HFSCs

To investigate the molecular mechanisms underlying fasting-induced HFSC death, we purified HFSCs from control and fasted animals during early anagen using fluorescence-activated cell sorting (FACS). To best capture common gene changes associated with HFSCs apoptosis *in vivo*, we subjected mice to 24 or 48 h of fasting, then dissociated the back skin and FACS-sorted HFSCs directly into Trizol for RNA sequencing (RNA-seq) analysis (Figures 6A and S6A–S6C). Ingenuity pathway analysis (IPA) was conducted to identify major changes in molecular pathways (Figure 6B). We observed downregulation of the glycolysis pathway and upregulation of the fatty acid metabolism pathway in fasted HFSCs, confirming their transition from utilizing glucose to FFAs (Figure 6C). Notably, apart from alterations related to cellular metabolism, the most prominent changes in fasted HFSCs were those associated with oxidative stress response, mitochondrial dysfunction, and apoptosis pathways (Figures 6D, S6D, and S6E). These findings suggest that fasting-induced HFSC apoptosis may be associated with heightened cellular oxidative stress.

(F) Ultrastructure of HFSCs. Pseudo-coloring indicates normal HFSCs (green) and apoptotic HFSCs (red). White arrowheads mark the damaged mitochondria in fasted HFSC (blue box).
(G) 8-oxoG staining of HFs after 24-h fasting (n = 3).
(H) Heatmaps of signature antioxidant gene expression in HFSCs and EpiSCs.
(I) Topical application of vitamin E (VE), or genetic overexpression of catalase (CAT OE), rescued HFSC apoptosis upon fasting.
(J) Hair regrowth of mice receiving VE or CAT OE under ADF (n = 3–5). Data are presented as mean ± SEM.
Scale bars, 500 nm (F), 30 μm (G and I).
See also Figure S6.

Please cite this article in press as: Chen et al., Intermittent fasting triggers interorgan communication to suppress hair follicle regeneration, Cell (2025), https://doi.org/10.1016/j.cell.2024.11.004

As cellular oxidative stress usually arises from increased production of reactive oxygen species (ROS), we employed MitoSox mitochondrial superoxide indicators to measure the levels of mitochondrial ROS in fasted HFSCs. A substantial rise in MitoSox signals was detected in HFSCs following 24 h of fasting, suggesting elevated mitochondrial ROS (Figure 6E). Elevated mitochondrial ROS, without effective antioxidant mechanisms, can damage components of the respiratory chain in mitochondria. This leads to the release of more free radicals, initiating a vicious cycle that results in oxidative stress and apoptosis.[59] To confirm the mitochondrial damage and oxidative stress in fasted HFSCs, we utilize tetramethylrhodamine, methyl ester (TMRM), to measure mitochondrial membrane potential in fasted HFSCs. A dramatic decrease in TMRM signals was observed in fasted HFSCs, indicating mitochondrial dysfunction (Figure 6E). In addition, transmission electron microscopy identified degenerated mitochondrial cristae in fasted HFSCs, a feature of damaged mitochondria (Figure 6F, white arrowheads). Furthermore, 8-oxoguanine (8-oxoG) staining revealed elevated oxidative DNA damage in fasted HFSCs, indicating heightened cellular oxidative stress in the stem cells (Figure 6G). These data suggest that fasting-induced apoptosis of HFSCs is associated with activated FAO and increased production of ROS, causing oxidative damage and apoptosis.

In mice undergoing long-term intermittent fasting for 6 months, elevated 8-oxoG signals could also be detected in the HFSC compartment (Figure S6F). RNA-seq analysis revealed similar upregulation of fatty acid metabolism and oxidative stress pathways in these HFSCs (Figure S6G). Notably, levels of 8-isoprostane, a marker of systemic oxidative stress, were reduced in the blood of these mice (Figure S6H), aligning with previous observations in human studies.[1,3] This discrepancy indicates that changes in HFSCs' cellular oxidative stress levels during intermittent fasting do not align with changes in systemic oxidative stress levels of the body. Furthermore, these HFSCs showed increased expression of genes associated with the Wnt signaling pathway and cell cycle progression, likely because some hair follicles were still stuck in an early anagen stage (Figures S6I and S6J). While the number of stem cells decreases due to repeated activation and elimination (Figure 2I), the surviving HFSCs displayed reduced inflammatory markers, suppressed differentiation programs, and increased markers of stress resistance and DNA damage repair (Figure S6K). This is consistent with previous findings in other stem cell systems and human studies, suggesting that repetitive metabolic switching during intermittent fasting induces adaptive cellular stress response and may actively select for more resilient cells.[8,14,15] In aged skin, the dermal adipose layer expands, accompanied by elevated 8-oxoG signals in the activated HFSCs (Figures S6L and S6M). Additionally, apoptotic HFSCs were observed in some hair follicles even without fasting (Figure S6N), likely caused by heightened oxidative stress.

Enhancement of antioxidant capability prevents fasting-induced HFSC death

In contrast to the glycolysis pathway normally employed by activated HFSCs,[20] FAO inherently generates more ROS from the electron transport chain leakage.[60] Indeed, blocking FAO in HFSCs using *Lhx2*^{CreER}; *Cpt1a*$^{fl/fl}$ mice alleviated fasting-induced HFSC death (Figure 4I). Because oxidative stress often occurs when cellular ROS production outweighs antioxidant capacity,[61] we postulated that the lack of effective antioxidant mechanisms in activated HFSCs could be the underlying reason for their apoptosis when transitioning to FAO upon fasting. To test this hypothesis, we FACS-purified EpiSCs, which share the same lineage origin with HFSCs during development but are resistant to fasting-induced apoptosis (Figure S2N), directly into Trizol for RNA-seq analysis. We then compared their expression of genes encoding key antioxidant enzymes with HFSCs. Compared with EpiSCs, activated HFSCs have significantly lower expression levels of antioxidant genes (Figure 6H), making them more susceptible to ROS-induced damage. By contrast, quiescent HFSCs in telogen hair follicles, which are resistant to fasting-induced apoptosis, exhibited higher levels of antioxidant gene expression and lower oxidative damage upon fasting (Figures S6O and S6P). Based on these findings, we asked whether HFSC death can be alleviated by applying exogenous antioxidants. Topical application of antioxidant vitamin E to the skin, or genetic overexpression of a critical antioxidant enzyme catalase (CAT),[62] effectively prevented fasting-induced apoptosis of HFSCs and mitigated hair follicle regeneration inhibition in mice subjected to intermittent fasting (Figures 6I and 6J). Under AL, HFSC activation, lipolysis in dermal adipocytes, and hair cycle progression remain largely unaffected in these models (Figures S6Q–S6S). Taken together, our data indicate that extended fasting activates FAO in HFSCs, leading to increased cellular ROS production. Due to their limited antioxidant capacity, this results in oxidative damage in the stem cells and apoptosis. Enhancing the antioxidant capacity of HFSCs, either pharmacologically or genetically, effectively prevents stem cell death and mitigates regeneration defects.

Metabolic switching to FAO induces HFSC apoptosis and inhibits hair growth in humans

To determine whether utilizing FFAs also induces elevated ROS and apoptosis in human HFSCs, we purified HFSCs from the scalp hair follicles of healthy donors and treated them with FFAs[63,64] (Figure S7A). Elevated MitoSox signals were observed in human HFSCs following FFA treatment, indicating increased mitochondrial ROS levels (Figures 7A and S7B). Moreover, TMRM assays revealed heightened mitochondrial damage, and apoptosis detection assays indicated increased apoptosis in these HFSCs, consistent with our findings in mouse HFSCs (Figures 7A and 7B). To further support these findings, we established a human hair follicle explant model and performed similar FFA treatments. Evident apoptotic signals can be identified within human hair follicles where active cycling HFSCs and progenitor cells are located,[65,66] along with elevated 8-oxoG signals in these cells (Figures 7C and S7C). Together, these findings provide evidence that similar to mouse HFSCs, human HFSCs also experience increased ROS production and subsequent mitochondria dysfunction, eventually undergoing apoptosis when switching to utilizing FFAs.

To determine whether intermittent fasting affects hair growth in humans, we conducted a human randomized controlled trial (RCT) study (Westlake Precision Nutrition Study 2,

Please cite this article in press as: Chen et al., Intermittent fasting triggers interorgan communication to suppress hair follicle regeneration, Cell (2025), https://doi.org/10.1016/j.cell.2024.11.004

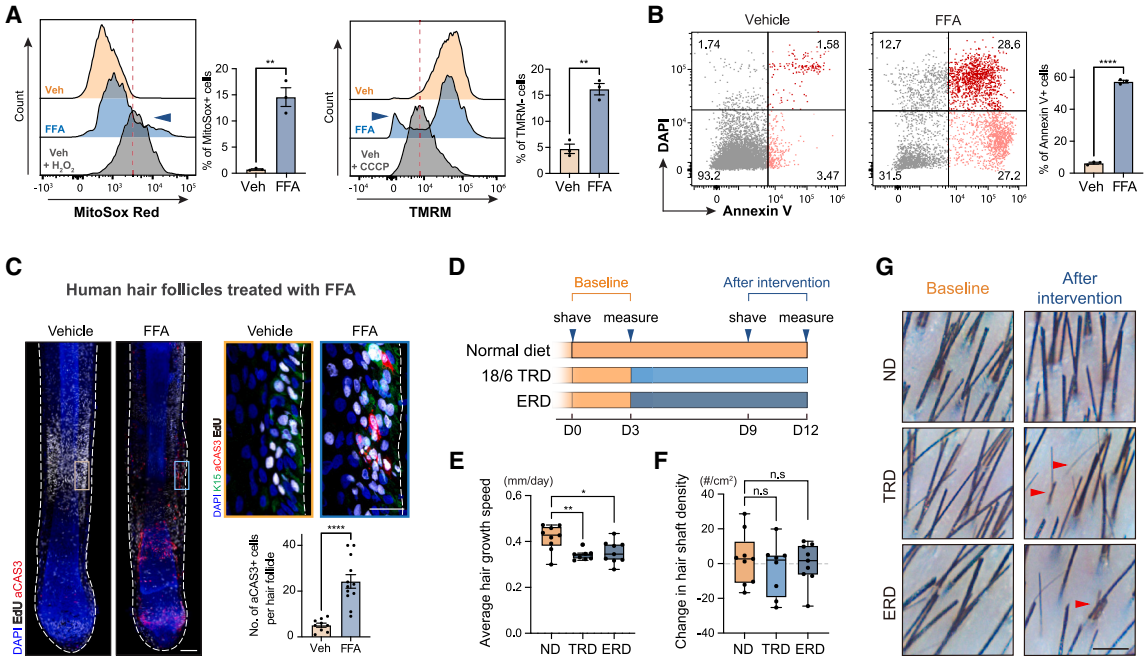

Figure 7. Metabolic switching to FAO induces HFSC apoptosis and inhibits hair growth in humans

(A) MitoSox and TMRM measurement in human HFSCs treated with FFA (n = 3).

(B) Analysis of apoptosis in human HFSCs treated with FFA using annexin V/DAPI apoptosis detection kit (n = 3).

(C) Left: whole-mount staining for EdU and aCAS3 of cultured human HFs treated with FFA or vehicle. Right top, staining for aCAS3, keratin 15 (K15, a marker for human HFSC), and EdU of human HFs treated with FFA or vehicle (n = 9–12 HFs, two-tailed unpaired t test).

(D) Schematic of dietary intervention in the Weprecision-2 human RCT study.

(E) Average hair growth speed (millimeter per day) in the last 3 days of intervention.

(F) Changes in hair shaft density after intervention.

(G) Hairs regrown 3 days post-shaving during baseline or intervention periods. Red arrowheads mark the abnormal hair shafts. Scale bars, 100 μm (C, left), 30 μm (C, right), 1 mm (G). In the bar graph, data are presented as mean ± SEM. In the box plot, data are presented as the interquartile range and median. *p < 0.05, **p < 0.01, ****p < 0.0001, n.s., not significant.

See also Figure S7 and Tables S1 and S2.

Clinicaltrials.gov NCT05800730). The primary outcome assessed the effects of intermittent fasting on glycemic homeostasis, while changes in hair growth were measured as a secondary outcome. Recruitment of the first participant began on April 14, 2023, and the study started on May 8 and concluded on May 19, 2023. 49 healthy young adults comprising both males and females were randomized to the 18/6 time-restricted diet (TRD), the energy restriction diet (ERD, 1,200–1,500 kcal/day), and a control group with a normal diet (ND, regular meal without timing restrictions; Figures S7D and S7E; Table S1; supplemental information). Consistent with previous findings,[1,3] intermittent fasting improved metabolic health (Figures S7F–S7I). To identify changes in hair growth, we shaved the existing hair within a 1 cm^2 area on the scalp and then measured the length of hair regrown back after 3 days. This experiment was conducted at both the baseline period and at the end of the intervention period (Figure 7D). Consistent with our findings in preclinical models, human participants undergoing intermittent fasting showed a significant inhibitory effect on hair growth—the average speed of hair growth in the TRD group decreased by 18% compared with the control group (p = 0.0028, Figures 7E and S7J). While hair shaft density did not show significant changes, many regrown hairs became shorter and thinner in diameter (Figures 7F, 7G, and S7K; Table S2). Moreover, as observed in mice, 18 h of fasting increases levels of lipolytic hormones in the blood of human participants following 18/6 TRD (Figure S7L), indicating that the systemic-level mechanisms mediating intermittent fasting's effect on HFSCs and hair growth are likely shared in humans.

DISCUSSION

Intermittent fasting offers a flexible and attractive alternative to conventional calorie restriction for weight management and metabolic health improvement. Here, our findings uncover its previously overlooked inhibitory effects on tissue regeneration in the skin. In mammals, fasting triggers evolutionarily conserved adaptative responses at both physiological and cellular levels that are vital for survival, with adrenal glands playing a pivotal role in the process.[53,54,57,67,68] In this study, we identified close interorgan communication between adrenal glands and niche adipocytes during intermittent fasting, which functions to eliminate activated somatic stem cells and disrupt the normal tissue regeneration process. As

Please cite this article in press as: Chen et al., Intermittent fasting triggers interorgan communication to suppress hair follicle regeneration, Cell (2025), https://doi.org/10.1016/j.cell.2024.11.004

adipocytes are common niche components for many stem cell systems, we postulated that this crosstalk may impact other tissue regeneration processes as well. During evolution, both wild animals and our human ancestors faced environments with fluctuating food availability, making fasting a regular occurrence. Our identified mechanism may enable them to halt peripheral tissue regeneration to conserve resources for more critical organs like the brain, thereby promoting adaptation and survival.

Previous studies have shown that activated adrenal glands affect stem cells through other niche cells. During chronic stress, corticosterone produced by the adrenal glands acts on the dermal papilla, inhibiting the activation of HFSCs and causing the hair follicle to remain in a prolonged telogen phase.[31] Fasting also stimulates the sympathetic nervous system, promoting the body's fitness behaviors and physiological adaptive responses. Nevertheless, ablation of sympathetic nerves does not prevent fasting-induced lipolysis in niche adipocytes and apoptosis in HFSCs. This contrasts with the role of sympathetic nerves in cold-temperature adaptation, where their activation promotes the activation of quiescent HFSCs and enhances hair growth.[30] Additionally, during acute stress, hyperactivation of sympathetic nerves in the skin can ectopically activate quiescent McSCs, depleting the stem cell pool and leading to gray hairs.[52] The differing responses of stem cells and tissue regeneration to adrenal and sympathetic activation in various contexts may be related to different intensities, durations, and patterns of stimuli, as well as to the specific characteristics of stem cells and the organization of their niches.[12] These complexities and variabilities may enable tissue regeneration processes to respond differently to diverse physiological and environmental changes.

The beneficial effects of intermittent fasting on body health are believed to stem from the periodic switching of metabolic fuel sources, which help optimize cellular energy utilization and induce adaptive cellular stress response.[8] This response enhances the expression of antioxidant defense and repair mechanisms, inhibits protein synthesis, and reduces cellular inflammation.[69–71] While similar responses were observed in HFSCs upon intermittent fasting, the activated HFSCs were selectively eliminated during the extended fasting periods, leading to inhibited hair follicle regeneration. Moreover, long-term intermittent fasting decreases the stem cell pool and induces hair follicle degeneration. Notably, fasting selectively harms HFSCs, but not EpiSCs, that maintain the epidermis with vital barrier functions. Previous studies have shown that in the gut, fasting and refeeding enhance intestinal stem cell function and intestinal epithelial repair,[14,72] while in the muscle, fasting induces the muscle stem cells to enter a deep quiescent status and delays muscle regeneration upon injury.[15] These observations suggest that the effects of fasting on various tissues and stem cell systems are likely context-dependent and require careful examination. Here, we demonstrated that the inherent variations in EpiSCs and HFSCs' antioxidant capacities are crucial for their distinct responses to fasting. While previous studies and our own data both indicated that intermittent fasting reduces markers of whole-body oxidative stress levels in circulation,[1,3] for activated HFSCs with limited endogenous antioxidant capacity and thus primarily rely on glycolysis for energy production, switching to utilizing FFAs during fasting increases their cellular ROS production, leading to increased cellular oxidative damage and apoptosis. This discrepancy in oxidative stress level changes between HFSCs and the whole-body underscores the unique metabolic demands and specific microenvironments ("niches") of these stem cells. As tissue regeneration is a resource-demanding process, one potential explanation for the divergence in response to fasting among different stem cell populations and tissue types could be that it allows the body to allocate limited resources toward preserving essential organ systems for survival, such as the intestine for nutrient absorption and the skin epidermis for barrier function. Importantly, we show that enhancing HFSCs' antioxidant ability through the external supply of antioxidants can significantly alleviate the inhibitory effect of intermittent fasting on hair follicle regeneration, offering a promising strategy for counteracting its impact on hair growth in humans.

Our study suggests that the basic principles and mechanisms underlying the effects of intermittent fasting on HFSCs are likely conserved between mice and humans. However, significant differences in metabolism, physiology, and hair follicle biology between the two species may account for the varying severity of the effects observed. For example, rodents have a higher metabolic rate and respond more rapidly to fasting, which likely facilitates faster and more robust metabolic switching during intermittent fasting, causing a stronger inhibitory effect on hair follicle regeneration and hair growth compared with humans. Additionally, mouse hair follicles predominantly stay in the telogen phase and transition to anagen for hair growth. Eliminating activated HFSCs prevents the hair follicle from growing further to produce hair shafts. By contrast, around 90% of human scalp hair follicles normally stay in anagen. Apoptosis of activated HFSCs and progenitor cells in these hair follicles leads to slower and defective hair shaft production, just as we have observed in human participants under the 18/6 TRD.

In conclusion, our findings illustrate the principles and mechanisms through which intermittent fasting profoundly influences somatic stem cells and tissue biology and delineate a comprehensive strategy for studying such impacts. Considering the widespread adoption of intermittent fasting globally, in the future, it will be important to thoroughly assess the effects of various fasting regimens on different stem cell systems. Understanding the complexity of responses across different stem cells and tissues is critical for optimizing these intervention strategies in humans and exploring ways to mitigate any unintended effects on tissue biology while retaining their benefits.

Limitations of the study

This study has several limitations. First, while we have demonstrated that activated HFSCs in aged skin exhibit elevated oxidative damage, the exact relationship between fasting-induced and age-related HFSC apoptosis requires further investigation. Second, due to challenges in acquiring material, whether FAO induces apoptosis in early anagen human hair follicles was not tested. Third, our human RCT study was conducted exclusively on healthy young adults and did not include

individuals with obesity, where intermittent fasting regimens are commonly adopted. Additionally, the long-term effects of intermittent fasting on hair growth and hair shaft density were not evaluated, as this was outside the predefined scope of the study.

RESOURCE AVAILABILITY

Lead contact

Further information and requests for resources and reagents should be directed to and will be fulfilled by the lead contact, Bing Zhang (zhangbing@westlake.edu.cn).

Materials availability

All unique reagents generated in this study are available from the lead contact.

Data and code availability

No original codes were generated in this study. The sequencing data are available from GEO: GSE246952. Any additional information required to reanalyze the data reported in this paper is available from the lead contact upon request.

ACKNOWLEDGMENTS

We thank Y.-C. Hsu, Q. Ma, D. He, D. Li, Y. Ge, and T. Chen for discussions on the manuscript; the Laboratory Animal Resources Center, Mass Spectrometry & Metabolomics Core Facility, High-Performance Computing Center, Flow Cytometry Core, Genomic Core, and Microscopy Core at Westlake University for technical support; and T. Chen and E. Fuchs for the K14-H2BGFP mice. This work was supported in part by grants from the National Natural Science Foundation of China (project 32170850 to B.Z.), the Key R&D Program of Zhejiang (2024SSYS0031), the Westlake Laboratory of Life Sciences and Biomedicine, the Research Center for Industries of the Future (RCIF), and the Center of Synthetic Biology and Integrated Bioengineering at Westlake University.

AUTHOR CONTRIBUTIONS

H. Chen, C.L., and S.C. performed most of the experiments. Y.X. performed the MitoSox assay and TEM. C.L., S.C., K.Z., and J.-S.Z. conducted the human RCT. H. Cheng and J.Z. isolated human hair follicles. J.P. made the initial observations of hair growth delay in fasted mice and performed RNA-seq experiments. X.Y. performed bioinformatic analysis. L.L. analyzed hair follicles from mice under chronic intermittent fasting. H.Y. performed the sympathetic ganglia staining. B.Z. wrote the manuscript with feedback from all co-authors.

DECLARATION OF INTERESTS

The authors declare no competing interests.

STAR★METHODS

Detailed methods are provided in the online version of this paper and include the following:

SUPPLEMENTAL INFORMATION

Supplemental information can be found online at https://doi.org/10.1016/j.cell.2024.11.004.

Received: January 28, 2024
Revised: August 29, 2024
Accepted: November 6, 2024
Published: December 13, 2024

REFERENCES

1. Sutton, E.F., Beyl, R., Early, K.S., Cefalu, W.T., Ravussin, E., and Peterson, C.M. (2018). Early time-restricted feeding improves insulin sensitivity, blood pressure, and oxidative stress even without weight loss in men with prediabetes. Cell Metab. *27*, 1212–1221.e3. https://doi.org/10.1016/j.cmet.2018.04.010.
2. Mitchell, S.J., Bernier, M., Mattison, J.A., Aon, M.A., Kaiser, T.A., Anson, R.M., Ikeno, Y., Anderson, R.M., Ingram, D.K., and de Cabo, R. (2019). Daily fasting improves health and survival in male mice independent of diet composition and calories. Cell Metab. *29*, 221–228.e3. https://doi.org/10.1016/j.cmet.2018.08.011.
3. Cienfuegos, S., Gabel, K., Kalam, F., Ezpeleta, M., Wiseman, E., Pavlou, V., Lin, S., Oliveira, M.L., and Varady, K.A. (2020). Effects of 4- and 6-h Time-Restricted Feeding on Weight and cardiometabolic Health: A randomized controlled trial in Adults with Obesity. Cell Metab. *32*, 366–378.e3. https://doi.org/10.1016/j.cmet.2020.06.018.
4. Hepler, C., Weidemann, B.J., Waldeck, N.J., Marcheva, B., Cedernaes, J., Thorne, A.K., Kobayashi, Y., Nozawa, R., Newman, M.V., Gao, P., et al. (2022). Time-restricted feeding mitigates obesity through adipocyte thermogenesis. Science *378*, 276–284. https://doi.org/10.1126/science.abl8007.
5. Cheng, C.-W., and Yilmaz, Ö.H. (2021). 100 years of exploiting diet and nutrition for tissue regeneration. Cell Stem Cell *28*, 370–373. https://doi.org/10.1016/j.stem.2021.02.014.
6. Di Francesco, A., Di Germanio, C., Bernier, M., and de Cabo, R. (2018). A time to fast. Science *362*, 770–775. https://doi.org/10.1126/science.aau2095.
7. Longo, V.D., and Panda, S. (2016). Fasting, circadian rhythms, and time-restricted feeding in healthy lifespan. Cell Metab. *23*, 1048–1059. https://doi.org/10.1016/j.cmet.2016.06.001.
8. de Cabo, R., and Mattson, M.P. (2019). Effects of intermittent fasting on health, aging, and disease. N. Engl. J. Med. *381*, 2541–2551. https://doi.org/10.1056/NEJMra1905136.

9. Brandhorst, S., Choi, I.Y., Wei, M., Cheng, C.W., Sedrakyan, S., Navarrete, G., Dubeau, L., Yap, L.P., Park, R., Vinciguerra, M., et al. (2015). A periodic diet that mimics fasting promotes multi-system regeneration, enhanced cognitive performance, and healthspan. Cell Metab. *22*, 86–99. https://doi.org/10.1016/j.cmet.2015.05.012.

10. Scadden, D.T. (2006). The stem-cell niche as an entity of action. Nature *441*, 1075–1079. https://doi.org/10.1038/nature04957.

11. Hsu, Y.-C., and Fuchs, E. (2012). A family business: stem cell progeny join the niche to regulate homeostasis. Nat. Rev. Mol. Cell Biol. *13*, 103–114. https://doi.org/10.1038/nrm3272.

12. Zhang, B., and Chen, T. (2024). Local and systemic mechanisms that control the hair follicle stem cell niche. Nat. Rev. Mol. Cell Biol. *25*, 87–100. https://doi.org/10.1038/s41580-023-00662-3.

13. Mana, M.D., Kuo, E.Y.-S., and Yilmaz, Ö.H. (2017). Dietary regulation of adult stem cells. Curr. Stem Cell Rep. *3*, 1–8. https://doi.org/10.1007/s40778-017-0072-x.

14. Mihaylova, M.M., Cheng, C.-W., Cao, A.Q., Tripathi, S., Mana, M.D., Bauer-Rowe, K.E., Abu-Remaileh, M., Clavain, L., Erdemir, A., Lewis, C.A., et al. (2018). Fasting activates fatty acid oxidation to enhance intestinal stem cell function during homeostasis and aging. Cell Stem Cell *22*, 769–778.e4. https://doi.org/10.1016/j.stem.2018.04.001.

15. Benjamin, D.I., Both, P., Benjamin, J.S., Nutter, C.W., Tan, J.H., Kang, J., Machado, L.A., Klein, J.D.D., de Morree, A., Kim, S., et al. (2022). Fasting induces a highly resilient deep quiescent state in muscle stem cells via ketone body signaling. Cell Metab. *34*, 902–918.e6. https://doi.org/10.1016/j.cmet.2022.04.012.

16. Cheng, C.-W., Adams, G.B., Perin, L., Wei, M., Zhou, X., Lam, B.S., Da Sacco, S., Mirisola, M., Quinn, D.I., Dorff, T.B., et al. (2014). Prolonged fasting reduces IGF-1/PKA to promote hematopoietic-stem-cell-based regeneration and reverse immunosuppression. Cell Stem Cell *14*, 810–823. https://doi.org/10.1016/j.stem.2014.04.014.

17. Chandel, N.S., Jasper, H., Ho, T.T., and Passegué, E. (2016). Metabolic regulation of stem cell function in tissue homeostasis and organismal ageing. Nat. Cell Biol. *18*, 823–832. https://doi.org/10.1038/ncb3385.

18. Shapira, S.N., and Christofk, H.R. (2020). Metabolic regulation of tissue stem cells. Trends Cell Biol. *30*, 566–576. https://doi.org/10.1016/j.tcb.2020.04.004.

19. Meacham, C.E., DeVilbiss, A.W., and Morrison, S.J. (2022). Metabolic regulation of somatic stem cells in vivo. Nat. Rev. Mol. Cell Biol. *23*, 428–443. https://doi.org/10.1038/s41580-022-00462-1.

20. Flores, A., Schell, J., Krall, A.S., Jelinek, D., Miranda, M., Grigorian, M., Braas, D., White, A.C., Zhou, J.L., Graham, N.A., et al. (2017). Lactate dehydrogenase activity drives hair follicle stem cell activation. Nat. Cell Biol. *19*, 1017–1026. https://doi.org/10.1038/ncb3575.

21. Kim, C.S., Ding, X., Allmeroth, K., Biggs, L.C., Kolenc, O.I., L'Hoest, N., Chacón-Martínez, C.A., Edlich-Muth, C., Giavalisco, P., Quinn, K.P., et al. (2020). Glutamine metabolism controls stem cell fate reversibility and long-term maintenance in the hair follicle. Cell Metab. *32*, 629–642.e8. https://doi.org/10.1016/j.cmet.2020.08.011.

22. Morris, R.J., and Potten, C.S. (1999). Highly persistent label-retaining cells in the hair follicles of mice and their fate following induction of anagen. J. Invest. Dermatol. *112*, 470–475. https://doi.org/10.1046/j.1523-1747.1999.00537.x.

23. Paus, R., and Cotsarelis, G. (1999). The biology of hair follicles. N. Engl. J. Med. *341*, 491–497. https://doi.org/10.1056/NEJM199908123410706.

24. Greco, V., Chen, T., Rendl, M., Schober, M., Pasolli, H.A., Stokes, N., dela Cruz-Racelis, J., and Fuchs, E. (2009). A two-step mechanism for stem cell activation during hair regeneration. Cell Stem Cell *4*, 155–169. https://doi.org/10.1016/j.stem.2008.12.009.

25. Cotsarelis, G., Sun, T.-T., and Lavker, R.M. (1990). Label-retaining cells reside in the bulge area of pilosebaceous unit: implications for follicular stem cells, hair cycle, and skin carcinogenesis. Cell *61*, 1329–1337. https://doi.org/10.1016/0092-8674(90)90696-C.

26. Blanpain, C., Lowry, W.E., Geoghegan, A., Polak, L., and Fuchs, E. (2004). Self-renewal, multipotency, and the existence of two cell populations within an epithelial stem cell niche. Cell *118*, 635–648. https://doi.org/10.1016/j.cell.2004.08.012.

27. Tumbar, T., Guasch, G., Greco, V., Blanpain, C., Lowry, W.E., Rendl, M., and Fuchs, E. (2004). Defining the epithelial stem cell niche in skin. Science *303*, 359–363. https://doi.org/10.1126/science.1092436.

28. Hsu, Y.-C., Li, L., and Fuchs, E. (2014). Emerging interactions between skin stem cells and their niches. Nat. Med. *20*, 847–856. https://doi.org/10.1038/nm.3643.

29. Joost, S., Annusver, K., Jacob, T., Sun, X., Dalessandri, T., Sivan, U., Sequeira, I., Sandberg, R., and Kasper, M. (2020). The molecular anatomy of mouse skin during hair growth and rest. Cell Stem Cell *26*, 441–457.e7. https://doi.org/10.1016/j.stem.2020.01.012.

30. Shwartz, Y., Gonzalez-Celeiro, M., Chen, C.-L., Pasolli, H.A., Sheu, S.-H., Fan, S.M.-Y., Shamsi, F., Assaad, S., Lin, E.T.-Y., Zhang, B., et al. (2020). Cell types promoting goosebumps form a niche to regulate hair follicle stem cells. Cell *182*, 578–593.e19. https://doi.org/10.1016/j.cell.2020.06.031.

31. Choi, S., Zhang, B., Ma, S., Gonzalez-Celeiro, M., Stein, D., Jin, X., Kim, S.T., Kang, Y.-L., Besnard, A., Rezza, A., et al. (2021). Corticosterone inhibits GAS6 to govern hair follicle stem-cell quiescence. Nature *592*, 428–432. https://doi.org/10.1038/s41586-021-03417-2.

32. Rooth, G., and Carlström, S. (1970). Therapeutic fasting. Acta Med. Scand. *187*, 455–463. https://doi.org/10.1111/j.0954-6820.1970.tb02970.x.

33. Goette, D.K., and Odom, R.B. (1976). Alopecia in crash dieters. JAMA *235*, 2622–2623.

34. Chaix, A., Lin, T., Le, H.D., Chang, M.W., and Panda, S. (2019). Time-restricted feeding prevents obesity and metabolic syndrome in mice lacking a circadian clock. Cell Metab. *29*, 303–319.e4. https://doi.org/10.1016/j.cmet.2018.08.004.

35. Anson, R.M., Guo, Z., de Cabo, R., Iyun, T., Rios, M., Hagepanos, A., Ingram, D.K., Lane, M.A., and Mattson, M.P. (2003). Intermittent fasting dissociates beneficial effects of dietary restriction on glucose metabolism and neuronal resistance to injury from calorie intake. Proc. Natl. Acad. Sci. USA *100*, 6216–6220. https://doi.org/10.1073/pnas.1035720100.

36. Zhang, B., and Hsu, Y.-C. (2017). Emerging roles of transit-amplifying cells in tissue regeneration and cancer. Wiley Interdiscip. Rev. Dev. Biol. *6*. https://doi.org/10.1002/wdev.282.

37. Wang, L., Siegenthaler, J.A., Dowell, R.D., and Yi, R. (2016). Foxc1 reinforces quiescence in self-renewing hair follicle stem cells. Science *351*, 613–617. https://doi.org/10.1126/science.aad5440.

38. Hsu, Y.-C., Pasolli, H.A., and Fuchs, E. (2011). Dynamics between stem cells, niche, and progeny in the hair follicle. Cell *144*, 92–105. https://doi.org/10.1016/j.cell.2010.11.049.

39. Zhang, C., Wang, D., Wang, J., Wang, L., Qiu, W., Kume, T., Dowell, R., and Yi, R. (2021). Escape of hair follicle stem cells causes stem cell exhaustion during aging. Nat Aging *1*, 889–903. https://doi.org/10.1038/s43587-021-00103-w.

40. Liu, G.Y., and Sabatini, D.M. (2020). mTOR at the nexus of nutrition, growth, ageing and disease. Nat. Rev. Mol. Cell Biol. *21*, 183–203. https://doi.org/10.1038/s41580-019-0199-y.

41. Deng, Z., Lei, X., Zhang, X., Zhang, H., Liu, S., Chen, Q., Hu, H., Wang, X., Ning, L., Cao, Y., et al. (2015). mTOR signaling promotes stem cell activation via counterbalancing BMP-mediated suppression during hair regeneration. J. Mol. Cell Biol. *7*, 62–72. https://doi.org/10.1093/jmcb/mjv005.

42. Yilmaz, Ö.H., Katajisto, P., Lamming, D.W., Gültekin, Y., Bauer-Rowe, K.E., SenGupta, S., Birsoy, K., Dursun, A., Yilmaz, V.O., Selig, M., et al. (2012). mTORC1 in the Paneth cell niche couples intestinal stem-cell function to calorie intake. Nature *486*, 490–495. https://doi.org/10.1038/nature11163.

43. Cahill, G.F. (1970). Starvation in Man. N. Engl. J. Med. *282*, 668–675. https://doi.org/10.1056/NEJM197003192821209.

44. Jensen, M.D., Haymond, M.W., Gerich, J.E., Cryer, P.E., and Miles, J.M. (1987). Lipolysis during fasting. Decreased suppression by insulin and increased stimulation by epinephrine. J. Clin. Invest. *79*, 207–213. https://doi.org/10.1172/JCI112785.

45. Jensen, T.L., Kiersgaard, M.K., Sørensen, D.B., and Mikkelsen, L.F. (2013). Fasting of mice: a review. Lab Anim. *47*, 225–240. https://doi.org/10.1177/0023677213501659.

46. Longo, V.D., and Mattson, M.P. (2014). Fasting: molecular mechanisms and clinical applications. Cell Metab. *19*, 181–192. https://doi.org/10.1016/j.cmet.2013.12.008.

47. Festa, E., Fretz, J., Berry, R., Schmidt, B., Rodeheffer, M., Horowitz, M., and Horsley, V. (2011). Adipocyte lineage cells contribute to the skin stem cell niche to drive hair cycling. Cell *146*, 761–771. https://doi.org/10.1016/j.cell.2011.07.019.

48. Zhang, B., Tsai, P.-C., Gonzalez-Celeiro, M., Chung, O., Boumard, B., Perdigoto, C.N., Ezhkova, E., and Hsu, Y.-C. (2016). Hair follicles' transit-amplifying cells govern concurrent dermal adipocyte production through Sonic Hedgehog. Genes Dev. *30*, 2325–2338. https://doi.org/10.1101/gad.285429.116.

49. Grabner, G.F., Xie, H., Schweiger, M., and Zechner, R. (2021). Lipolysis: cellular mechanisms for lipid mobilization from fat stores. Nat. Metab. *3*, 1445–1465. https://doi.org/10.1038/s42255-021-00493-6.

50. Sipe, L.M., Yang, C., Ephrem, J., Garren, E., Hirsh, J., and Deppmann, C.D. (2017). Differential sympathetic outflow to adipose depots is required for visceral fat loss in response to calorie restriction. Nutr. Diabetes *7*, e260. https://doi.org/10.1038/nutd.2017.13.

51. Sheng, M., and Greenberg, M.E. (1990). The regulation and function of c-fos and other immediate early genes in the nervous system. Neuron *4*, 477–485. https://doi.org/10.1016/0896-6273(90)90106-P.

52. Zhang, B., Ma, S., Rachmin, I., He, M., Baral, P., Choi, S., Gonçalves, W.A., Shwartz, Y., Fast, E.M., Su, Y., et al. (2020). Hyperactivation of sympathetic nerves drives depletion of melanocyte stem cells. Nature *577*, 676–681. https://doi.org/10.1038/s41586-020-1935-3.

53. Djurhuus, C.B., Gravholt, C.H., Nielsen, S., Mengel, A., Christiansen, J.S., Schmitz, O.E., and Møller, N. (2002). Effects of cortisol on lipolysis and regional interstitial glycerol levels in humans. Am. J. Physiol. Endocrinol. Metab. *283*, E172–E177. https://doi.org/10.1152/ajpendo.00544.2001.

54. Kim, B.H., Joo, Y., Kim, M.-S., Choe, H.K., Tong, Q., and Kwon, O. (2021). Effects of intermittent fasting on the circulating levels and circadian rhythms of hormones. Endocrinol. Metab. *36*, 745–756. https://doi.org/10.3803/EnM.2021.405.

55. Ahima, R.S., Prabakaran, D., Mantzoros, C., Qu, D., Lowell, B., Maratos-Flier, E., and Flier, J.S. (1996). Role of leptin in the neuroendocrine response to fasting. Nature *382*, 250–252. https://doi.org/10.1038/382250a0.

56. Perry, R.J., Wang, Y., Cline, G.W., Rabin-Court, A., Song, J.D., Dufour, S., Zhang, X.M., Petersen, K.F., and Shulman, G.I. (2018). Leptin mediates a glucose-fatty acid cycle to maintain glucose homeostasis in starvation. Cell *172*, 234–248.e17. https://doi.org/10.1016/j.cell.2017.12.001.

57. Douglass, A.M., Resch, J.M., Madara, J.C., Kucukdereli, H., Yizhar, O., Grama, A., Yamagata, M., Yang, Z., and Lowell, B.B. (2023). Neural basis for fasting activation of the hypothalamic–pituitary–adrenal axis. Nature *620*, 154–162. https://doi.org/10.1038/s41586-023-06358-0.

58. Shook, B.A., Wasko, R.R., Mano, O., Rutenberg-Schoenberg, M., Rudolph, M.C., Zirak, B., Rivera-Gonzalez, G.C., López-Giráldez, F., Zarini, S., Rezza, A., et al. (2020). Dermal adipocyte lipolysis and myofibroblast conversion are required for efficient skin repair. Cell Stem Cell *26*, 880–895.e6. https://doi.org/10.1016/j.stem.2020.03.013.

59. Redza-Dutordoir, M., and Averill-Bates, D.A. (2016). Activation of apoptosis signalling pathways by reactive oxygen species. Biochim. Biophys. Acta *1863*, 2977–2992. https://doi.org/10.1016/j.bbamcr.2016.09.012.

60. Bigarella, C.L., Liang, R., and Ghaffari, S. (2014). Stem cells and the impact of ROS signaling. Development *141*, 4206–4218. https://doi.org/10.1242/dev.107086.

61. Halliwell, B. (2023). Understanding mechanisms of antioxidant action in health and disease. Nat. Rev. Mol. Cell Biol. *25*, 13–33. https://doi.org/10.1038/s41580-023-00645-4.

62. Schriner, S.E., Linford, N.J., Martin, G.M., Treuting, P., Ogburn, C.E., Emond, M., Coskun, P.E., Ladiges, W., Wolf, N., Van Remmen, H., et al. (2005). Extension of murine life span by overexpression of catalase targeted to mitochondria. Science *308*, 1909–1911. https://doi.org/10.1126/science.1106653.

63. Kageyama, T., Miyata, H., Seo, J., Nanmo, A., and Fukuda, J. (2023). In vitro hair follicle growth model for drug testing. Sci. Rep. *13*, 4847. https://doi.org/10.1038/s41598-023-31842-y.

64. Beyaz, S., Mana, M.D., Roper, J., Kedrin, D., Saadatpour, A., Hong, S.-J., Bauer-Rowe, K.E., Xifaras, M.E., Akkad, A., Arias, E., et al. (2016). High-fat diet enhances stemness and tumorigenicity of intestinal progenitors. Nature *531*, 53–58. https://doi.org/10.1038/nature17173.

65. Rochat, A., Kobayashi, K., and Barrandon, Y. (1994). Location of stem cells of human hair follicles by clonal analysis. Cell *76*, 1063–1073. https://doi.org/10.1016/0092-8674(94)90383-2.

66. Inoue, K., Aoi, N., Sato, T., Yamauchi, Y., Suga, H., Eto, H., Kato, H., Araki, J., and Yoshimura, K. (2009). Differential expression of stem-cell-associated markers in human hair follicle epithelial cells. Lab. Invest. *89*, 844–856. https://doi.org/10.1038/labinvest.2009.48.

67. Pasiakos, S.M., Caruso, C.M., Kellogg, M.D., Kramer, F.M., and Lieberman, H.R. (2011). Appetite and endocrine regulators of energy balance after 2 days of energy restriction: insulin, leptin, ghrelin, and DHEA-S. Obesity (Silver Spring) *19*, 1124–1130. https://doi.org/10.1038/oby.2010.316.

68. Steinhauser, M.L., Olenchock, B.A., O'Keefe, J., Lun, M., Pierce, K.A., Lee, H., Pantano, L., Klibanski, A., Shulman, G.I., Clish, C.B., et al. (2018). The circulating metabolome of human starvation. JCI Insight *3*, e121434. https://doi.org/10.1172/jci.insight.121434.

69. Randle, P.J., Garland, P.B., Hales, C.N., and Newsholme, E.A. (1963). The glucose fatty-acid cycle its role in insulin sensitivity and the metabolic disturbances of diabetes mellitus. Lancet *1*, 785–789. https://doi.org/10.1016/S0140-6736(63)91500-9.

70. Anton, S.D., Moehl, K., Donahoo, W.T., Marosi, K., Lee, S.A., Mainous, A.G., Leeuwenburgh, C., and Mattson, M.P. (2018). Flipping the metabolic switch: understanding and applying health benefits of fasting. Obesity (Silver Spring) *26*, 254–268. https://doi.org/10.1002/oby.22065.

71. Mattson, M.P., Moehl, K., Ghena, N., Schmaedick, M., and Cheng, A. (2018). Intermittent metabolic switching, neuroplasticity and brain health. Nat. Rev. Neurosci. *19*, 63–80. https://doi.org/10.1038/nrn.2017.156.

72. Imada, S., Khawaled, S., Shin, H., Meckelmann, S.W., Whittaker, C.A., Corrêa, R.O., Alquati, C., Lu, Y., Tie, G., Pradhan, D., et al. (2024). Short-term post-fast refeeding enhances intestinal stemness via polyamines. Nature *633*, 895–904. https://doi.org/10.1038/s41586-024-07840-z.

73. Li, X., Yu, B., Sun, Q., Zhang, Y., Ren, M., Zhang, X., Li, A., Yuan, J., Madisen, L., Luo, Q., et al. (2018). Generation of a whole-brain atlas for the cholinergic system and mesoscopic projectome analysis of basal forebrain cholinergic neurons. Proc Natl Acad Sci U S A *115*, 415–420. https://doi.org/10.1073/pnas.1703601115.

74. Schindelin, J., Arganda-Carreras, I., Frise, E., Kaynig, V., Longair, M., Pietzsch, T., Preibisch, S., Rueden, C., Saalfeld, S., Schmid, B., et al. (2012). Fiji: an open-source platform for biological-image analysis. Nature Methods *9*, 676–682. https://doi.org/10.1038/nmeth.2019.

75. Chen, S., Zhou, Y., Chen, Y., and Gu, J. (2018). fastp: an ultra-fast all-in-one FASTQ preprocessor. Bioinformatics *34*, i884–i890. https://doi.org/10.1093/bioinformatics/bty560.

76. Patro, R., Duggal, G., Love, M.I., Irizarry, R.A., and Kingsford, C. (2017). Salmon provides fast and bias-aware quantification of transcript expression. Nat. Methods *14*, 417–419. https://doi.org/10.1038/nmeth.4197.

77. Love, M.I., Huber, W., and Anders, S. (2014). Moderated estimation of fold change and dispersion for RNA-seq data with DESeq2. Genome Biol. *15*, 550. https://doi.org/10.1186/s13059-014-0550-8.

78. Russell, B.C., Torralba, A., Murphy, K.P., and Freeman, W.T. (2008). LabelMe: A database and web-based tool for image annotation. Int. J. Comput. Vision *77*, 157–173. https://doi.org/10.1007/s11263-007-0090-8.

79. Rowland, N.E. (2007). Food or fluid restriction in common laboratory animals: balancing welfare considerations with scientific inquiry. Comp. Med. *57*, 149–160.

80. Meng, J.-J., Shen, J.-W., Li, G., Ouyang, C.-J., Hu, J.-X., Li, Z.-S., Zhao, H., Shi, Y.-M., Zhang, M., Liu, R., et al. (2023). Light modulates glucose metabolism by a retina-hypothalamus-brown adipose tissue axis. Cell *186*, 398–412.e17. https://doi.org/10.1016/j.cell.2022.12.024.

81. Xu, Z., Chen, D., Hu, Y., Jiang, K., Huang, H., Du, Y., Wu, W., Wang, J., Sui, J., Wang, W., et al. (2022). Anatomically distinct fibroblast subsets determine skin autoimmune patterns. Nature *601*, 118–124. https://doi.org/10.1038/s41586-021-04221-8.

82. Bodó, E., Bíró, T., Telek, A., Czifra, G., Griger, Z., Tóth, B.I., Mescalchin, A., Ito, T., Bettermann, A., Kovács, L., et al. (2005). A hot new twist to hair biology: involvement of vanilloid Receptor-1 (VR1/TRPV1) signaling in human hair growth control. Am. J. Pathol. *166*, 985–998. https://doi.org/10.1016/S0002-9440(10)62320-6.

83. Sinclair, R., Jolley, D., Mallari, R., Magee, J., Tosti, A., Piracinni, B.M., Vincenzi, C., Happle, R., Ferrando, J., Grimalt, R., et al. (2003). Morphological approach to hair disorders. J. Investig. Dermatol. Symp. Proc. *8*, 56–64. https://doi.org/10.1046/j.1523-1747.2003.12172.x.

84. Chang, W.C., Chen, K.Y., Cheng, S.Y., Hsu, C.K., and Yang, C.C. (2023). Mapping the hair density, thickness, and volume in normal and androgenetic alopecia subjects with the digital microscope. JEADV Clin. Pract. *2*, 174–178. https://doi.org/10.1002/jvc2.86.

85. American Diabetes Association Professional; Practice Committee (2023). Diagnosis and classification of diabetes: standards of care in diabetes. Diabetes Care *47*, S20–S42. https://doi.org/10.2337/dc24-S002.

Please cite this article in press as: Chen et al., Intermittent fasting triggers interorgan communication to suppress hair follicle regeneration, Cell (2025), https://doi.org/10.1016/j.cell.2024.11.004

STAR★METHODS

KEY RESOURCES TABLE

REAGENT or RESOURCE	SOURCE	IDENTIFIER
Antibodies		
Rabbit polyclonal anti Perilipin-1	Abcam	Cat#ab3526; RRID: AB_2167274
Rat monoclonal anti Integrin alpha 6	eBioscience	Cat#14-0495-85; RRID: AB_891484
Rabbit polyclonal anti Cleaved caspase-3	Cell Signaling Technology	Cat#9661S; RRID: AB_2341188
Polyclonal Goat anti P-Cad	R&D Systems	Cat#AF761; RRID: AB_355581
Rat anti Krt6	Dr. T. Chen	N/A
Chicken polyclonal anti Krt14	Biolegend	Cat#906004; RRID: AB_2616962
Chicken polyclonal anti Krt15	Biolegend	Cat#833904; RRID: AB_2616894
Rat monoclonal anti CD45	eBioscience	Cat#14-0451-85; RRID: AB_467252
Goat polyclonal anti CD140a	R&D Systems	Cat#AF1062; RRID: AB_2236897
Rabbit monoclonal anti COL17A1	Abcam	Cat#ab186415; RRID: AB_3665723
Rabbit polyclonal anti TH	Millipore Sigma	Cat#AB152; RRID: AB_390204
Rabbit polyclonal anti c-FOS	Abcam	Cat#ab190289; RRID: AB_2737414
Mouse monoclonal anti 8-Oxoguanine	Abcam	Cat#ab62623; RRID: AB_940049
Rat monoclonal anti CD34	eBioscience	Cat#14-0341-85; RRID: AB_467211
Rabbit monoclonal anti GR	Cell Signaling Technology	Cat#3660T; RRID: AB_11179215
Rabbit polyclonal anti CPT1A	Proteintech	Cat#15184-1-AP; RRID: AB_2084676
Rabbit polyclonal anti TSC2	Proteintech	Cat#24601-1-AP; RRID: AB_2879633
Rabbit polyclonal anti ATGL	Proteintech	Cat#55190-1-AP; RRID: AB_11182818
Goat polyclonal anti Ephrin-B1	R&D systems	Cat#BAF473; RRID: AB_2293418
Rabbit polyclonal anti TSC2	Absin	Cat#abs148958; RRID: AB_3206290
Rabbit monoclonal anti β-Actin	Cell Signaling Technology	Cat#4970; RRID: AB_2223172
Guinea Pig anti DCT	HUABIO	custom-made
Rabbit polyclonal anti Ki67	Abcam	Cat#ab15580; RRID: AB_443209
FACS- alpha6-PE-Cy7	eBioscience	Cat#25-0495-82; RRID: AB_10804881
FACS- CD34-EF660	eBioscience	Cat#50-0341-82; RRID: AB_10596826
FACS- CD45-Biotin	eBioscience	Cat#13-0451-82; RRID: AB_466446
FACS- CD140a-Biotin	eBioscience	Cat#13-1401-82; RRID: AB_466607
FACS- Sca1-PerCP-Cy5.5	eBioscience	Cat#45-5981-82; RRID: AB_914372
Chemicals, peptides, and recombinant proteins		
Tamoxifen	Sigma-Aldrich	Cat#T5648
RU486	TCI	Cat#M1732
Palmitic acid	Sigma	Cat#P0500
Sodium oleate	Sigma	Cat#O7501
Benzyl alcohol	Shanghai yuanye Bio-Technology	Cat#S24194
Benzyl benzoate	Shanghai yuanye Bio-Technology	Cat#S24209
6-hydroxydopamine hydrobromide	Sigma-Aldrich	Cat#162957
Ascorbic acid	Sigma	Cat#A92902
Epinephrine	MedChemExpress	Cat#B0447B
Corticosterone	MedChemExpress	Cat#B1618
Propranolol hydrochloride	MedChemExpress	Cat#B0573
Vitamin E	Selleck	Cat#S4686
Glycerol	Sigma-Aldrich	Cat#G5516
Optimal cutting temperature	Sakura Finetek	Cat#4583
Neutral balsam mounting medium	BBI	Cat#E675007-0100

(*Continued on next page*)

Please cite this article in press as: Chen et al., Intermittent fasting triggers interorgan communication to suppress hair follicle regeneration, Cell (2025), https://doi.org/10.1016/j.cell.2024.11.004

Continued

REAGENT or RESOURCE	SOURCE	IDENTIFIER
Collagenase I	Worthington	Cat#LS004196
Collagenase II	Gibco	Cat#17101015
Collagenase IV	Worthington	Cat#LS004189
DNase I	Roche	Cat#11284932001
Fetal bovine serum	Sigma-Aldrich	Cat#F8318
0.25% Trypsin-EDTA	Gibco	Cat#2520056
HBSS	Thermo Fisher	Cat#24020117
Dispase II solution	STEM CELL	Cat#7913
MitoSox-Red	Invitrogen	Cat#M36008
TMRM	Invitrogen	Cat#M20036
CCCP	Invitrogen	Cat#M20036
Hydrogen peroxide solution	Aladdin	Cat#H112515
Palmitic acid	CAYMAN CHEMICAL	Cat#10006627
Williams E medium	Gibco	Cat#12551032
L-glutamine	Sigma-Aldrich	Cat#G8540
Hydrocortisone	MedChemExpress	Cat#HY-N0583
Insulin	MedChemExpress	Cat#HY-P0035
Antibiotics	MACKLIN	Cat#A6533
A8301	Tocris	Cat#379762
DMH-1	Tocris	Cat#813305
Y27632	Tocris	Cat#1254/10
Telaglenastat (CB839)	MedChemExpress	Cat#HY-12248
DMEM low glucose	Gibco	Cat#10567014
DAPI	Sigma	Cat#D9542
Protease inhibitor cocktail	MedChemExpress	Cat#HY-K0010
4%-12% gradient SDS-PAGE gel	Haoke	Cat#HKW3G42015
0.25% Trypsin-noEDTA	MEILUNBIO	Cat#PWL061
Cell Staining Buffer	BioLegend	Cat#422201
Annexin V Binding Buffer	BioLegend	Cat#420201
BODIPY	Invitrogen	Cat#D3922
Glutaraldehyde	TedPella	Cat#18426
Paraformaldehyde	TedPella	Cat#18505
Cacodylate buffer	Wako	Cat#036-8175
Osmium tetroxide	TedPella	Cat#18465
Uranyl acetate	Electron Microscopy Sciences	Cat #22400
PE Annexin V	BioLegend	Cat#640908
Critical commercial assays		
Corticosterone ELISA kit	Enzo Life Sciences	Cat#ADI-900-097
Epinephrine ELISA Kit	Abnova	Cat#KA1882
Leptin ELISA kit	Elabscience	Cat#E-MSEL-M0033
8-epi-PGF2α(8-Epi-Prostaglandin F2 Alpha) ELISA Kit	Elabscience	Cat#E-EL-0041
Cortisol Parameter Assay Kit	R&D systems	Cat#KGE008B
Free Fatty Acid Quantitation Kit	Sigma-Aldrich	Cat#MAK044
RNeasy Plus Micro Kit	Qiagen	Cat#74034
Single Cell Full Length mRNA-Amplification Kit	Vazyme	Cat#N712
TruePrep DNA Library Prep Kit V2 for Illumina	Vazyme	Cat#TD503

(*Continued on next page*)

Please cite this article in press as: Chen et al., Intermittent fasting triggers interorgan communication to suppress hair follicle regeneration, Cell (2025), https://doi.org/10.1016/j.cell.2024.11.004

Continued

REAGENT or RESOURCE	SOURCE	IDENTIFIER
Click-iT™ Plus EdU Flow Cytometry Assay Kits	Invitrogen	Cat#C10632
PrimeScript™ RT Master Mix kit	Takara	Cat#RR036A
Click-iT™ EdU Alexa Fluor™ 488 Imaging Kit	Invitrogen	Cat#C10337
Deposited data		
Bulk RNA-seq data	This paper	GEO: GSE246952
Experimental models: Organisms/strains		
Mouse: C57BL/6J	The Jackson Laboratory	JAX: 000664
Mouse: B6;SJL-Tg(Krt1-15-cre/PGR*) 22Cot/J	The Jackson Laboratory	JAX: 005249
Mouse: B6.129-Tg(Adipoq-cre/Esr1*) 1Evdr/J	The Jackson Laboratory	JAX: 024671
Mouse: B6.Cg-Dbh$^{tm3.2(cre)Pjen}$/J	The Jackson Laboratory	JAX: 033951
Mouse: B6(129S4)-Cpt1a^{em1Fink}/J	The Jackson Laboratory	JAX: 035711
Mouse: B6N.129S-Pnpla2^{tm1Eek}/J	The Jackson Laboratory	JAX: 024278
Mouse: B6.Cg-Tg(CAG-OTC/CAT) 4033Prab/J	The Jackson Laboratory	JAX: 016197
Mouse: C57BL/6Smoc-Tsc2$^{tm1(flox)Smoc}$	Shanghai Model Organisms Center, Inc.	RRID: IMSR_NM-CKO-2102032
Mouse: K14-H2BGFP	Tumbar et al.[27]	N/A
Mouse: B6.Cg-Nr3c1$^{tm1.1Jda}$/J	The Jackson Laboratory	JAX:021021
B6.Cg-Gt(ROSA)26Sor$^{tm9(CAG-tdTomato)Hze}$/J	The Jackson Laboratory	JAX: 007909
Mouse: Gt(ROSA)26Sor$^{tm47(CAG-EGFP*)Hze}$	Li et al.[73]	MGI:5750793
Mouse: Gt(ROSA) 26Sor$^{tm4(ACTB-tdTomato,-EGFP)Luo}$/J	The Jackson Laboratory	JAX: 007576
Mouse: Lhx2$^{tm1.1(cre/ERT2)Zjh}$/J	The Jackson Laboratory	JAX: 036293
Oligonucleotides		
Primer: Pnpla2 Forward: GGATGGCGGCATTTCAGACA	PrimerBank	26327465a1
Primer: Pnpla2 Reverse: CAAAGGGTTGGGTTGGTTCAG	PrimerBank	26327465a1
Primer: Lipe Forward: CCAGCCTGAGGGCTTACTG	PrimerBank	26325924a1
Primer: Lipe Reverse: CTCCATTGACTGTGACATCTCG	PrimerBank	26325924a1
Primer: Beta actin Forward: GGCTGTATTCCCCTCCATCG	PrimerBank	6671509a1
Primer: Beta actin Reverse: CCAGTTGGTAACAATGCCATGT	PrimerBank	6671509a1
Primer: Tsc2 Forward: TGAATGCGGCCTCAACAATC	PrimerBank	86439986c2
Primer: Tsc2 Reverse: GACAGCCTTCCAAAGTGCCT	PrimerBank	86439986c2
Primer: Cpt1a Forward: CCATGAAGCCCTCAAACAGATC	This paper	N/A
Primer: Cpt1a Reverse: ATCACACCCACCACCACGATA	This paper	N/A

(*Continued on next page*)

Please cite this article in press as: Chen et al., Intermittent fasting triggers interorgan communication to suppress hair follicle regeneration, Cell (2025), https://doi.org/10.1016/j.cell.2024.11.004

Continued

REAGENT or RESOURCE	SOURCE	IDENTIFIER
Software and algorithms		
Fiji (ImageJ)	Schindelin et al.[74]	https://imagej.net/Fiji
Ingenuity Pathway Analysis	QIAGEN	https://digitalinsights.qiagen.com/products-overview/discovery-insights-portfolio/analysis-and-visualization/qiagen-ipa/
FlowJo	FlowJo, LLC	https://www.flowjo.com
GraphPad Prism	GraphPad Software, Inc	https://www.graphpad.com
fastp	Chen et al.[75]	https://github.com/OpenGene/fastp
Salmon	Patro et al.[76]	https://github.com/COMBINE-lab/salmon
DESeq2	Love et al.[77]	https://bioconductor.org/packages/release/bioc/html/DESeq2.html
Sable System Macro Interpreter	Sable Systems	https://www.sablesys.com/products/promethion-high-definition-room-calorimetry-system/promethion-software
R	The R Project for Statistical Computing	http://www.r-project.org
LabelMe	Russell et al.[78]	https://github.com/CSAILVision/LabelMeAnnotationTool

EXPERIMENTAL MODEL AND STUDY PARTICIPANT DETAILS

Animal studies

C57BL/6J, K15^{CrePGR}, AdipoQ^{CreERT}, Lhx2^{CreERT2}, Dbh^{Cre}, Cpt1a$^{fl/fl}$, Atgl$^{fl/fl}$, mCAT, GR$^{fl/fl}$, Rosa-TdTomato, and Rosa-mTmG mice were obtained from the Jackson Laboratory. Tsc2$^{fl/fl}$ mice were generated by Shanghai Model Organisms Center, Inc. K14-H2BGFP[27] mice were originally generated by E. Fuchs (The Rockefeller University) and provided by T. Chen (National Institute of Biological Sciences). Ai47 mice were generated by H. Zeng (Allen Institute for Brain Science) and provided by D. He (Westlake University). All experiments utilized balanced groups of adult male and female mice aged 3-10 weeks at the onset of the experiments unless otherwise specified. Age-matched littermates were used, and experiments were performed in parallel unless otherwise specified. Mice were maintained in an animal facility in specific-pathogen-free conditions at 22°C with humidity of 40% to 70% and a 12/12 light/dark cycle and were approved by the Institutional Animal Care and Use Committee guidelines of Westlake University (AP#23-077-ZB) and compiled with all relevant ethical regulations.

Human participants

Participants for Westlake Precision Nutrition Study 2, WePrecision-2, were recruited exclusively from the Westlake Precision Nutrition Study 1 (WePrecision-1) conducted in 2021. Among the 49 participants, the median age was 27 years (interquartile range 26, 31), with 46% male and 54% female. All participants identified as East Asian Chinese. The study protocol was approved by the Westlake University Ethics Committee (the WePrecision-2: No.20230306ZJS001), along with the registration on ClinicalTrials.gov (the WePrecision-2: NCT05800730). All research participants gave their written informed consent to participate in the trial. Inclusion criteria: adults aged 18 to 60 years; male or female; residents of Hangzhou with no travel plans for the next 3 months. Exclusion criteria: long-term chronic gastrointestinal diseases; taking immunosuppressants or antibiotics as daily medication within the last 3 months; diabetes; hypertension and cardiovascular diseases; craniocerebral trauma, cancer, liver disease, kidney disease, or other critical illness; history of corresponding surgery or medication; bulimia nervosa; post-traumatic stress disorder; chronic anxiety and depression or other critical neuronal disorder or history of relevant medication; pregnant or lactating; history of alcohol or drug addiction, or smoke above 15 cigarettes per day; concurrently participating in other clinical trials.

METHOD DETAILS

Mice intermittent fasting procedures

Mice under ad libitum (AL) feeding were given 24-hour access to a regular chow diet (19.4% crude protein, 6.2% crude fat (w/w), energy 3.7 Kcal/g), formulated according to LabDiet® 5K52 used by Jackson Laboratory. Fasting was achieved through food removal for a period as specified before switching to the regular chow diet.[45,79] For time-restricted feeding procedures, mice were fed within feeding windows of 3 hours (21/3 TRF), 5 hours (19/5 TRF), 8 hours (16/8 TRF), or 12 hours (12/12 TRF) each day starting from Zeitgeber Time (ZT) 12. For the alternate-day fasting procedure, mice were fasted for 24 hours starting from ZT12, followed by 24 hours of refeeding with a regular chow diet.

Please cite this article in press as: Chen et al., Intermittent fasting triggers interorgan communication to suppress hair follicle regeneration, Cell (2025), https://doi.org/10.1016/j.cell.2024.11.004

Quantification of mice hair regrowth

The back skin of the mice was shaved at the beginning of the experiments. Mice pictures were taken at regular intervals and analyzed using ImageJ (v.1.53q). The rate of hair regrowth was calculated as the ratio of the hairy skin area to the entire back skin area.

Metabolic cage analysis

Whole-body metabolic states were measured in individually housed mice using the Promethion Core metabolic cage system (Sable Systems). The lighting and environmental temperature conditions were maintained to replicate those in the home cages. The mice underwent 2-4 days of acclimatization, followed by data collection over 3-7 days. All data were extracted from the raw data with a 30-minute slice using Sable System Macro Interpreter v.2.47 software.

Glucose tolerance test

The glucose tolerance test (GTT) procedure was conducted following previously described protocols.[34,80] Briefly, Mice undergoing GTT were fasted for 16 hours prior to the test. During the test, each mouse was injected with one dose of glucose (20% glucose solution, 1 g/kg), and blood samples were collected from the tail vein nicks at 0, 15, 30, 60, 90, 120, 150, and 180 minutes post-injection. These blood samples were measured by Accu-Chek Performa meter (Roche). The area under the time curves (AUC) data was calculated based on the method described in previous research.[80] To summarize, we calculate the percent change of blood glucose compared to the baseline (time 0), and the AUC using the linear trapezoidal rule:

$$g_{time(i)} = \left[\left(G_{time(i)} / G_{time(0)} - 1\right) * 100\right]\%$$

$$AUC = \left[\sum_{i=1}^{n} \frac{g_{time(i)} + g_{time(i-1)}}{2} * \left(time_{(i)} - time_{(i-1)}\right)\right] \Big/ \left(time_{(n)} - time_{(0)}\right)$$

where $g_{time(i)}$ is the percent change in blood glucose, $G_{time(0)}$ is the glucose concentration at baseline and $G_{time(i)}$ is the glucose concentration at one of timepoints.

Drug treatments

For tamoxifen treatment, tamoxifen (Sigma-Aldrich, T5648) was prepared in corn oil at 20 mg/ml and injected intraperitoneally at 200mg/kg for 6–8 days. For RU486 treatment, 4% RU486 (TCI, M1732) was prepared in ethanol and applied topically for 10-12 days. For intradermal fatty acid injection, palmitic acid (PA, Sigma P0500) and sodium oleate (OA, Sigma O7501) were prepared with 40% PEG300, 5% Tween80, 53% saline, and 2% DMSO to a final concentration of 7.8 mM (PA) and 7.2 mM (OA). Mice were injected with a single dose of 50ul at early anagen (~P27), and skin samples were collected 8 hours after injection. Control mice received an equivalent volume of solvent. For the PA concentration gradient test, 1.6 mM, 3.9 mM, and 7.8 mM PA were injected intradermally in early anagen mice skin, and skin samples were collected 8 hours after injection. For ablation of sympathetic nerves, 6-hydroxydopamine hydrobromide (6-OHDA, Sigma-Aldrich, 162957) solution was prepared freshly by dissolving 6-OHDA in 0.1% ascorbic acid in 0.9% sterile NaCl. Mice were injected intraperitoneally with 6-OHDA at P21 (250 mg/kg body weight), P23, and P25 (100 mg/kg body weight). Control mice received an equivalent volume of vehicle (0.1% ascorbic acid in 0.9% sterile NaCl). For lipolytic hormones injection, epinephrine (MedChemExpress, B0447B) solution was prepared freshly by dissolving in 0.1% ascorbic acid in 0.9% sterile NaCl to a final concentration of 4 mM. Corticosterone (MedChemExpress, B1618) was dissolved in 0.45% SBE-β-CD and 0.1% ascorbic acid in 0.9% sterile NaCl to a final concentration of 10 mM. 50 μL of epinephrine or corticosterone were injected intradermally into experimental mice. Control mice received an equivalent volume of solvent. The injection sites were marked using water-resistant ink. Female mice were injected at early anagen (around P27), and the skin samples were collected 6 hours later. For the ADRB3 antagonist treatment, propranolol (MedChemExpress, HY-B0573) was dissolved in PBS at a concentration of 2 mg/mL. The mice were injected intradermally at 10 mg/kg after fasting for 12 hours, before being sacrificed after another 12-hour fasting. For antioxidant treatment, vitamin E (Selleck, S4686) was dissolved in glycerol (Sigma-Aldrich, G5516) at 20 mg/mL. The back skin of mice was shaved, and vitamin E was topically administered at 200mg/kg twice per day at ZT0 and ZT12. For the glutaminase-1 inhibitor treatment, CB-839 (telaglenastat, MedChemExpress, HY-12248) was dissolved in 70% PEG300 and 30% (20% SBE-β-CD in Saline) at a concentration of 4 mg/mL. The mice were injected intraperitoneally at 40 mg/kg every 12 hours during the 24-hour fasting period. For free fatty acid treatment of human HFSCs and hair follicles, palmitic acid (Sigma, P0500) was directly dissolved into the culture media at a concentration of 30 μM. The HFSCs or hair follicles were then treated for 24 hours before being subjected to flow cytometry analysis or immunofluorescence staining.

EdU administration

EdU (Invitrogen, C10337, dissolved in 0.9% NaCl, 25 mg/kg body weight) was administered by intraperitoneal injection 5 hours before harvesting unless otherwise specified. For the EdU tracing assay, mice undergoing ADF received intraperitoneal injections of EdU every 6 hours during a 24-hour feeding period.

Adrenalectomy

Adrenalectomy was performed as previously described.[31] In brief, mice were anesthetized by isoflurane. Small incisions were made above the adrenal gland on the back skin. Both adrenal glands were removed using curve forceps and ophthalmic scissors. Sham mice underwent the same procedures without removing the adrenal glands. Both ADX and sham mice had their drinking water supplemented with 0.9% saline to keep the salt balance. After a 4-day rest, hair shafts were removed by waxing in the ADX/Sham mice to initiate entry into the anagen phase. Following a two-day period after waxing, ADX/Sham mice were subjected to ADF.

Histology and immunohistochemistry

Mouse skin samples were fixed using 4% paraformaldehyde (PFA) for 15 min at room temperature, washed with PBS, and immersed in 30% sucrose overnight at 4 °C. Samples were then embedded in the optimal cutting temperature (OCT) compound (Sakura Finetek, 4583). For HE staining, the cryosections were stained by the hematoxylin solution for 2 min and the eosin solution for 5 min, and rinsed with PBS after each staining. Samples were dehydrated by immersing in a series of ethanol solutions with increasing concentrations (90%, 95%, 100%), each for 15-20 sec. Slides were then immersed in xylene for 5 min for clearing, followed by mounting with a neutral balsam mounting medium (BBI, E675007-0100). The pictures were captured by a motorized fluorescence microscope (Nikon, Ni-E). For immunohistochemistry, cryosections were fixed in 4% PFA for 2 min and washed with PBS and 0.1% Triton X-100 in PBS. Slides were then blocked using blocking buffer (5% donkey serum; 1% BSA, 2% cold water fish gelatin in 0.3% Triton X-100 in PBS) for 1 hour at room temperature, followed by staining with primary antibodies overnight at 4°C and secondary antibodies for 4 hours at room temperature. Whole-mount staining was performed as previously described.[81] In brief, the back skin was collected after Nair treatment. Skin samples were fixed in 4% paraformaldehyde/PBS for 1 hour and washed with PBS. Then the samples were stained using primary antibodies for 24 hours at room temperature and secondary antibodies overnight at room temperature. The samples were dehydrated successively using 25%, 50%, 75%, and then 100% methanol, followed by tissue clearing using benzyl alcohol and benzyl benzoate. For 8-Oxoguanine (8-oxoG) staining, 10-μm paraffin sections were used, and antigen retrieval was performed by boiled sodium citrate buffer (0.01M, pH 6.0) for 20 min, followed by standard immunohistochemistry procedures described above. Antibodies used: Perilipin-1 (rabbit, Abcam ab3526, 1:800), Integrin alpha 6 (rat, eBioscience 14-0495-85, 1:100), Cleaved caspase-3 (rabbit, Cell Signaling Technology, 9661S, 1:300), P-Cad (goat, R&D Systems, AF761,1:200), Krt6 (rat, 1:400), Krt15 (chicken, Biolegend, 833904, 1:300), Krt14 (chicken, Biolegend, 906004, 1:300), CD34 (rat, eBioscience, 14-0341-85, 1:400), CD45 (rat, eBioscience, 14-0451-82, 1:300), CD140a (goat, R&D Systems, AF1062, 1:400), COL17A1(rabbit, Abcam, ab186415, 1:400), TH (rabbit, Millipore Sigma, AB152, 1:1000), 8-Oxoguanine (mouse, Abcam, ab62623, 1:800), CPT1A (rabbit, Proteintech, 15184-1-AP, 1:200), TSC2 (rabbit, Proteintech, 24601-1-AP, 1:200), ATGL (rabbit, Proteintech, 55190-1-AP, 1:200), Ephrin-B1 (goat, R&D Systems, BAF473, 1:400), GR (rabbit, Cell Signaling Technology, 3660T, 1:1000), DCT (guinea pig, HUABIO, 1:1000), cFOS (Abcam, ab190289, 1:1000), Ki67 (rabbit, Abcam, ab15580, 1:200).

Imaging and imaging analysis

Florescent images were acquired using a Zeiss LSM 800 confocal microscope with ×20 or ×40 objective lenses. Images were presented as maximum intensity projection unless otherwise specified. For colocalization analysis, images were presented as a single z-stack. The number of cells was counted manually or by using ImageJ. For quantification of hair follicle sizes, 70-μm sections were used. The length of the hair follicle was determined by the straight-line distance from the bottom of the dermal papilla to the opening of the hair follicle, and the size of the bulge was measured as the area of the largest sagittal plane of the hair follicle bulge; both measured using ZEN blue software 2.6.

Transmission electron microscope

Mice were perfused transcardially (4% glutaraldehyde+2% paraformaldehyde) before harvesting skin samples. Skin tissues were then sliced into small pieces (1 mm*2mm) and fixed by 2.5% glutaraldehyde and 2% paraformaldehyde in cacodylate buffer at 4 °C. Skin pieces were then fixed in 1% osmium tetroxide for 90 min and stained with 1% uranyl acetate for 60 min at 4 °C. Fixed tissue was dehydrated using ascending grades of ethanol and transferred into the resin via acetone. After infiltration with pure resin, specimens were embedded in the same resin mixture. Ultra-thin sections (70 nm) were placed on copper grids and stained with 3% uranyl acetate for 30 min and Sato's lead for 3 min. Stained sections were observed with a 120kV Transmission Electron Microscope (Thermo Scientific, Talos L120C G2) operating at 80 kV.

Gas chromatography-mass spectrometry

Dermal adipocytes were isolated as previously described.[58] In brief, mice dorsal skin was digested using collagenase I and centrifuged at 300 g for 4 min. Floating adipocytes were collected and washed with PBS and snap-frozen in liquid nitrogen. Total lipid was extracted, and analysis was performed on an Agilent 7890B gas chromatography coupled with a 5977B mass spectrometer equipped with an electron impact ion source (Agilent Technologies, USA). The data processing was performed using the Agilent MassHuter workstation.

Measurement of hormones, blood glucose, and FFAs

For blood glucose measurement, blood was collected from a small tail cut, and the blood glucose was measured every 6 hours using the Accu-Chek Performa meter (Roche). For hormone measurement, whole blood was obtained from the orbital sinus of mice and collected into centrifuge tubes containing heparin sodium. Plasma was subsequently collected following centrifugation. Corticosterone ELISA kit (Enzo Life Sciences, ADI-900-097), Epinephrine ELISA Kit (Abnova, KA1882), Leptin ELISA kit (Elabscience, E-MSEL-M0033), and 8-epi-PGF2α ELISA Kit (Elabscience, E-EL-0041) were used according to the manufacturer's instructions. For FFAs measurement in the skin, skin biopsies were obtained using 6 mm biopsy punches. The tissues were homogenized in 1% (w/v) Triton X-100 in chloroform solution, followed by centrifugation at 13,000 g for 10 minutes to remove insoluble material. The organic phase (lower phase) was collected and air dried at 50°C to remove chloroform. Vacuum drying was used to remove trace chloroform and finally get the dried lipids sample. FFAs level was measured by the Free Fatty Acid Quantitation Kit (Sigma-Aldrich, MAK044).

Fluorescence-activated cell sorting

Mouse dorsal skin was dissected, diced into small pieces, and incubated in a digestion buffer consisting of 0.1% collagenase II (Gibco, 17101015), 0.2% collagenase IV (Worthington, LS004189), and 50 μg/ml DNase I (Roche, 11284932001) in a 5% FBS in PBS solution at 37 °C for 90 min on a shaker. After centrifugation, the pellets were digested using 0.25% Trypsin-EDTA (Gibco, 2520056) at 37 °C for 15 min. Single-cell suspension was obtained by filtering through 70-μm and 40-μm filters, centrifuged at 500g at 4 °C for 10 min, and resuspended in 5% FBS in PBS. The cells were stained with fluorescent dye-conjugated antibodies at 4 °C for 30 min. Antibodies used: alpha6-PE-Cy7 (eBioscience, 25-0495-82, 1:500), CD34-EF660 (eBioscience, 50-0341-82, 1:100), CD45-Biotin (eBioscience, 13-0451-82, 1:400), CD140a-Biotin (eBioscience, 13-1401-82, 1:200), Sca1-PerCP-Cy5.5 (eBioscience, 45-5981-82, 1:1000). DAPI (Sigma, D9542) was used to exclude dead cells. Cell isolation was performed with BD FACAria™ Fusion.

EdU flow cytometry assay

The EdU flow cytometry assay was performed according to the manufacturer's instructions (Click-iT™ Plus EdU Flow Cytometry Assay Kits, Invitrogen, C10632). Briefly, EdU (25 mg/kg) was injected 8 hours before harvesting skin samples. Skin cells were collected as described above. After staining with antibodies to identify HFSCs, the skin cells were fixed, permeabilized, and stained for EdU through the Click-iT reaction. EdU+ HFSCs proportions were then analyzed by flow cytometry.

Quantitative reverse-transcription PCR

The quantitative reverse-transcription PCR (RT-qPCR) was performed using PrimeScript™ RT Master Mix kit (Takara, RR036A) on a Bio-Rad CFX Connect Real-Time PCR Detection System. Ct values were normalized to an internal control of β-actin.

Western blot analysis

HFSC cells cultured in vitro were lysed using a RIPA buffer (containing 25 mM Tris, pH 7.4, 150 mM NaCl, 0.5% Na-deoxycholate, 0.1% SDS, and 1% Triton X-100) supplemented with a protease inhibitor cocktail (MCE, HY-K0010). The resultant protein extracts were separated using a 4%-12% gradient SDS-PAGE gel (Haoke, HKW3G42015). The separated proteins were transferred onto a nitrocellulose membrane, which was subsequently blocked using 5% non-fat milk. The target protein was detected using a primary antibody followed by an Alexa Fluor 647-conjugated secondary antibody.

Human hair follicle stem cell isolation and cell culture

The experiment was approved by the Westlake University Ethics Committee (Approval number: 20231217ZB001). Human hair follicle stem cell isolation was performed as previously described.[63] Briefly, human hair follicles were obtained using follicle unit extraction (FUE) techniques. The hair bulb was removed, and the remaining follicle tissue was digested in 4.8 U/mL Dispase II (STEM CELL, 7913) and 100 U/mL collagenase IV (Worthington, LS004189) in PBS for 60 minutes at 37°C. After the surgical removal of the hair shaft, the collagen sheath was treated with trypsin in PBS for another 60 minutes at 37°C. Following centrifugation, the isolated human hair follicle stem cells (HFSCs) were seeded in E-Medium supplemented with 1 μM A8301, 1 μM DMH-1, and 10 μM Y27632.

Human hair follicle tissue culture

The experiment was approved by the Westlake University Ethics Committee (Approval number: 20231217ZB001). The human hair follicle culture followed established protocols.[82] Briefly, human hair follicles were extracted using follicle unit extraction (FUE) techniques. The isolated hair follicles were cultured in 24-well plates using supplemented Williams E medium (Gibco, 12551032) containing 2 mM L-glutamine (Sigma-Aldrich, G8540-100G), 10 ng/mL hydrocortisone (MCE, HY-N0583), 10 μg/mL insulin (MCE, HY-P0035), and antibiotics (MACKLIN, A6533). The tissue was incubated at 37 °C, 5% CO_2 for 8 hours. The culture medium was further supplemented with 10 μM EdU and 30 μM of palmitic acid (CAYMAN CHEMICAL, 10006627). Following 24 hours of treatment, the hair follicle tissues were subjected to a whole-mount staining procedure.

MitoSox and TMRM assay

Single-cell suspension of mouse skin was prepared and stained with antibodies as above. Then the cells were resuspended with warm FBS/PBS buffer and incubated with 500 nM MitoSox-Red (Invitrogen, M36008) or 20 nM TMRM (Invitrogen, M20036) at 37 °C for 30 minutes on a shaker. 0.5 μM H_2O_2 or 10 μM CCCP (Invitrogen, M20036) was used as the positive control. The fluorescence was measured in the HFSC populations using flow cytometry analysis. For human HFSCs MitoSox staining and imaging, the HFSCs were isolated as above and plated into a glass-bottomed dish for MitoSox staining. When cell confluence reached 70%, palmitic acid was introduced into the culture media at a concentration of 30 μM. After 24 hours of treatment, MitoSox-Red was added to the culture media at a final concentration of 0.5 μM and incubated at 37 °C for 30 minutes. Then the cells were washed three times with Hank's Balanced Salt Solution (HBSS). The fluorescence images were captured using a Zeiss LSM 800 confocal microscope within 2 hours under the same parameters. ImageJ was used to quantify the integrated density.

Annexin V-FITC / DAPI apoptosis detection

Cultured HFSC cells were dissociated with 0.25% Trypsin-noEDTA (MEILUNBIO, PWL061). The dissociated cells (5×10⁵) were washed with Cell Staining Buffer (BioLegend, 422201). After being centrifuged at 500g at 4 °C, the cell pellet was resuspended in 400 μL of Annexin V Binding Buffer (BioLegend, 420201) that contained Annexin V (BioLegend, 640908, 1:3000 dilution) and 0.5 μg/mL DAPI (Sigma, D9542). The cell suspension was incubated at room temperature for 15 minutes. Cell apoptosis was subsequently assessed using flow cytometry.

Skin explant harvesting and treatment

The dorsal skin of mice was dissected after sterilization, and the subcutaneous muscle was gently removed. The skin containing dermal adipocytes was then cut into small pieces and cultured in a low-glucose medium at 37 °C with 5% CO2 for 3 hours. Following this incubation, the skin pieces were treated with hormones for 6 hours. Corticosterone was dissolved in the low-glucose DMEM medium (Gibco, 10567014) to achieve final concentrations of 0.1 μM, 1 μM, and 10 mM. Similarly, epinephrine was dissolved in the low-glucose medium to final concentrations of 0.2 nM, 2 nM, and 2 mM. After 6 hours of hormone treatment at 37 °C with 5% CO2, the skin samples were subjected to whole-mount staining as previously described.

RNA-seq and computational analysis

HFSCs (CD140a-; CD45-; Sca1-; CD34+; alpha6+) and EpiSCs (CD140a-; CD45-; Sca1+; CD34-; alpha6+) were isolated from fed and fasted mice at early anagen using FACS. RNA samples were purified using RNeasy Plus Micro Kit (Qiagen, 74034), and RNA-seq libraries were generated using Single Cell Full Length mRNA-Amplification Kit (Vazyme, N712) and TruePrep DNA Library Prep Kit V2 for Illumina (Vazyme, TD503). Paired-end sequencing reads were obtained using the Illumina NovaSeq 6000 platform. Sequencing reads from RNA-seq libraries were trimmed using fastp,[75] paired reads were removed if they contained over 10% N bases, over 50% low-quality (Q<=5) bases, or adapter sequences in any read. Trimmed reads were mapped to the mouse reference transcriptome (mm10) performing quantification using Salmon.[76] Gene expression levels were normalized and differential expression of genes was calculated using the DESeq2 package in R.[77] Pathway analysis was performed using QIAGEN Ingenuity Pathway Analysis (2023).

Randomized controlled trial for human hair growth analysis

The WePrecision-2 study was a dietary intervention trial conducted from May 8 to May 19, 2023. The 49 participants were randomly assigned to one of the three groups: normal diet (ND), time-restricted diet (TRD), and energy-restricted diet (ERD). Randomization was conducted by a researcher who was not involved in the recruitment and enrollment work. The primary outcome of this trial was to assess the effects of TRD and ERD on glycemic homeostasis, as measured by oral glucose tolerance tests (OGTT) and continuous glucose monitoring (CGM). The secondary outcome was to validate the impact of TRD and ERD on hair growth. Before the intervention started (day 3), the baseline hair growth speed (from day 0 to day 3) was measured. All participants were required to wear the continuous glucose monitor (CGM) on day 1, and the baseline physical examination was conducted on day 2. Between Day 3 and Day 12, ERD restricted daily total energy intake within 1200–1500 kcal but no dining circadian limits, while 18:6 TRD restricted the daily feeding window from 10:00 to 16:00 without total energy intake restriction. The ND group was instructed to maintain original eating habits for control. Out of the 49 participants, 35 completed the entire dietary intervention. Of these, hair growth measurements were available from 26 participants: 9 participants in the ND group, 8 participants in the TRD group (one of them was not available for fasting blood collection after intervention), and 9 participants in the ERD group.

Assessment of human hair growth, hair density, and metabolic traits

To assess hair growth, a 1 cm^2 area on the back of the scalp was shaved. Trichoscopy (Meiboyi, M-12) was used to capture hair shaft images. Hair length was measured manually and independently by two experimenters, who were blinded to group assignments using LabelMe software (version 5.3.1).[78] Measurements were repeated after 3 days to determine the speed of hair growth during this period. The average hair growth speed was assessed at both the baseline period (day 0 – day 3) and the end of the intervention period (day 9 – day 12). The hair shaft width was also measured, and the density of terminal hair (≥ 30 μm) and vellus hair (< 30 μm) were calculated as the number of hair shafts with roots present in the image, divided by the size of the image.[83,84] To assess the impact of

TRD and ERD on metabolic health indicators, serum samples were collected on days 2 (baseline) and day 13 (after intervention). The serum high-density lipoprotein (HDL) was determined on a Cobas c701 analyzer (Roche Diagnostics), and the low-density lipoprotein (LDL) was determined on a Cobas c502 analyzer (Roche Diagnostics). Connecting-peptide (c-peptide) was measured using chemiluminescent immunoassays on an Alinity i instrument (Abbott).

QUANTIFICATION AND STATISTICAL ANALYSIS

Power and sample size calculation in human trial

The 2-hour post-OGTT (oral glucose tolerance test) glucose level was used to determine the required sample size in the WePrecision-2 study. We estimated that the time-restricted diet (TRD) or energy-restricted diet (ERD) group could improve this glucose index by 30% of the clinically relevant difference (3.3 mmol/L between the diagnostic thresholds for diabetes and pre-diabetes),[85] equating to 1.0 mmol/L. Our previous WePrecision-1 study reported a mean OGTT-2h glucose level of 6.2 ± 1.3 mmol/L. Accordingly, we calculated that n = 13 participants per group would provide 80% power to detect a 1.0 mmol/L difference. With anticipating a dropout rate of 20%, we initially aimed to recruit 48 participants (n = 16 per group), assuming that 39 participants (n = 13 per group) would complete the trial. Post-hoc power analysis indicated that our trial has 92% power to detect the observed difference of 0.075 mm/day in hair growth between the TRD group (n = 8) and the control group (n = 9), with a significance level of 0.05 using two-sided two sample t-test.

Statistical Analyses

Statistical analyses were performed using GraphPad Prism and R. For comparisons between two groups, unpaired two-tailed Student's t-tests were used. For comparisons involving more than two groups, one-way ANOVA with Tukey's multiple comparisons test was employed. Two-way ANOVA with Dunnett's multiple comparisons test was utilized in cases requiring the analysis of two factors. * $P < 0.05$, ** $P < 0.01$, *** $P < 0.001$, **** $P < 0.0001$, n.s, not significant. In the bar graph, the data are presented as mean ± s.e.m. In the box plot, the data are presented as the interquartile range (IQR, the box), median (the line inside the box), and all individual data points. Center lines show the medians; box limits indicate the 25th and 75th percentiles; whiskers extend 1.5 times the interquartile range from the 25th and 75th percentiles.

ADDITIONAL RESOURCES

The registry information of the Westlake Precision Nutrition Study 2: ClinicalTrial #NCT05800730, https://classic.clinicaltrials.gov/ct2/show/NCT05800730.

CellPress

Supplemental figures

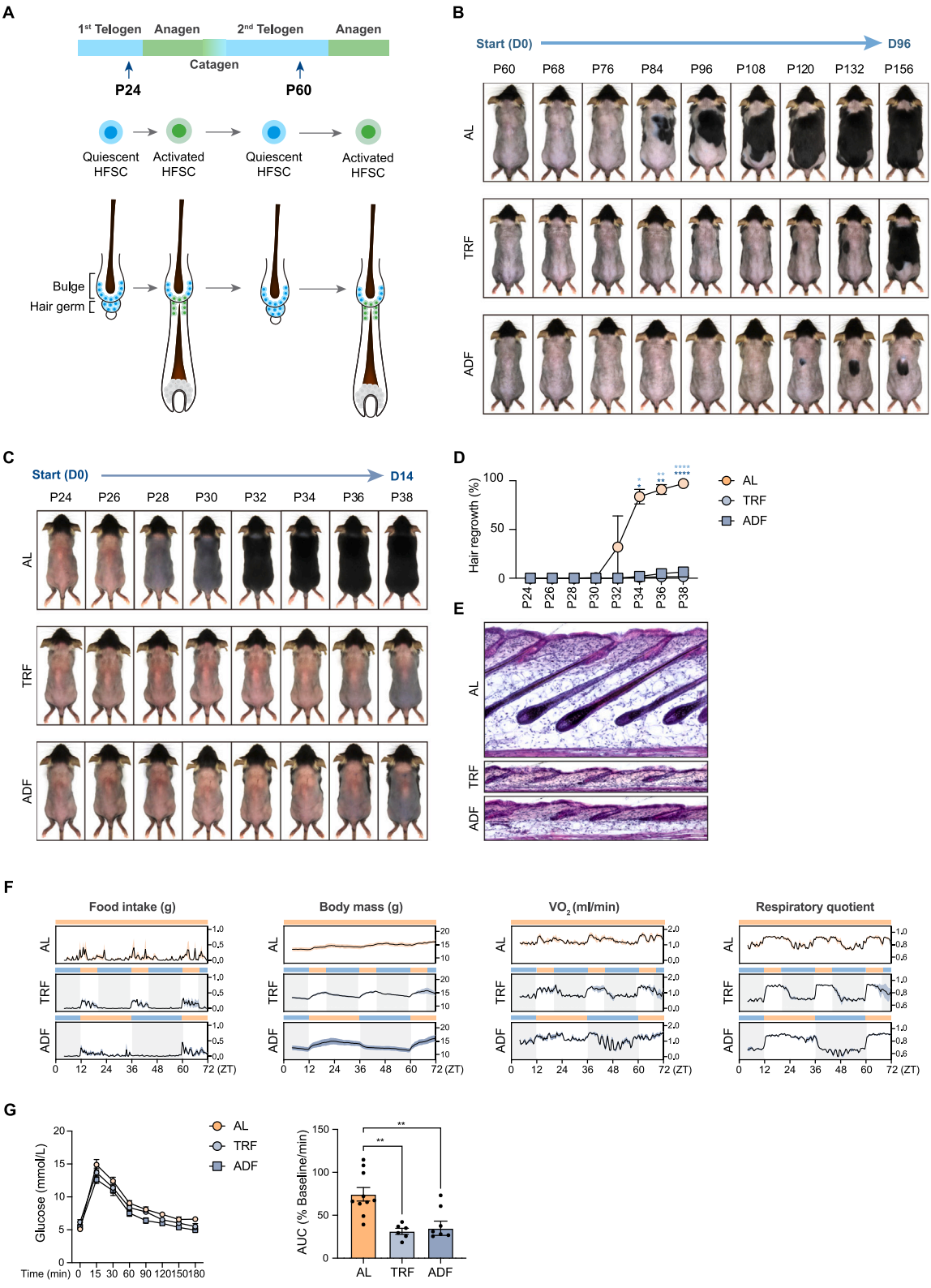

(legend on next page)

Figure S1. Intermittent fasting inhibits hair regeneration, related to Figure 1

(A) Schematic of mouse hair cycle phases driven by the periodic activation of HFSCs.

(B) Progression of hair regrowth in male mice subjected to AL, 16/8 TRF, and ADF paradigms between postnatal day (P) 60 and P156. Mice were shaved before treatments (representative images from 8 to 10 mice for each group are shown here).

(C) Progression of hair regrowth in female mice subjected to AL, 16/8 TRF, and ADF paradigms between P24 and P38. Mice were shaved before treatments (representative images from 6–8 mice for each group are shown here).

(D) Quantification of the hair regrowth in mice in (C) (n = 3 mice for each group, two-way analysis of variance [ANOVA] with Dunnett multiple comparisons test).

(E) H&E staining of skin from AL, TRF, and ADF mice in P34.

(F) Metabolic states of mice under AL, TRF, and ADF were measured by metabolic cages over a 72-h period starting from P26. Periods of fasting are shadowed by a blue color (n = 3 mice for each group).

(G) Glucose tolerance test in mice under AL, TRF, and ADF paradigms for 6 months (n = 6–10 mice for each group). AUC, area under the time curves. Scale bar, 100 μm. Data are presented as mean ± SEM. *p < 0.05, **p < 0.01, ****p < 0.0001, n.s., not significant.

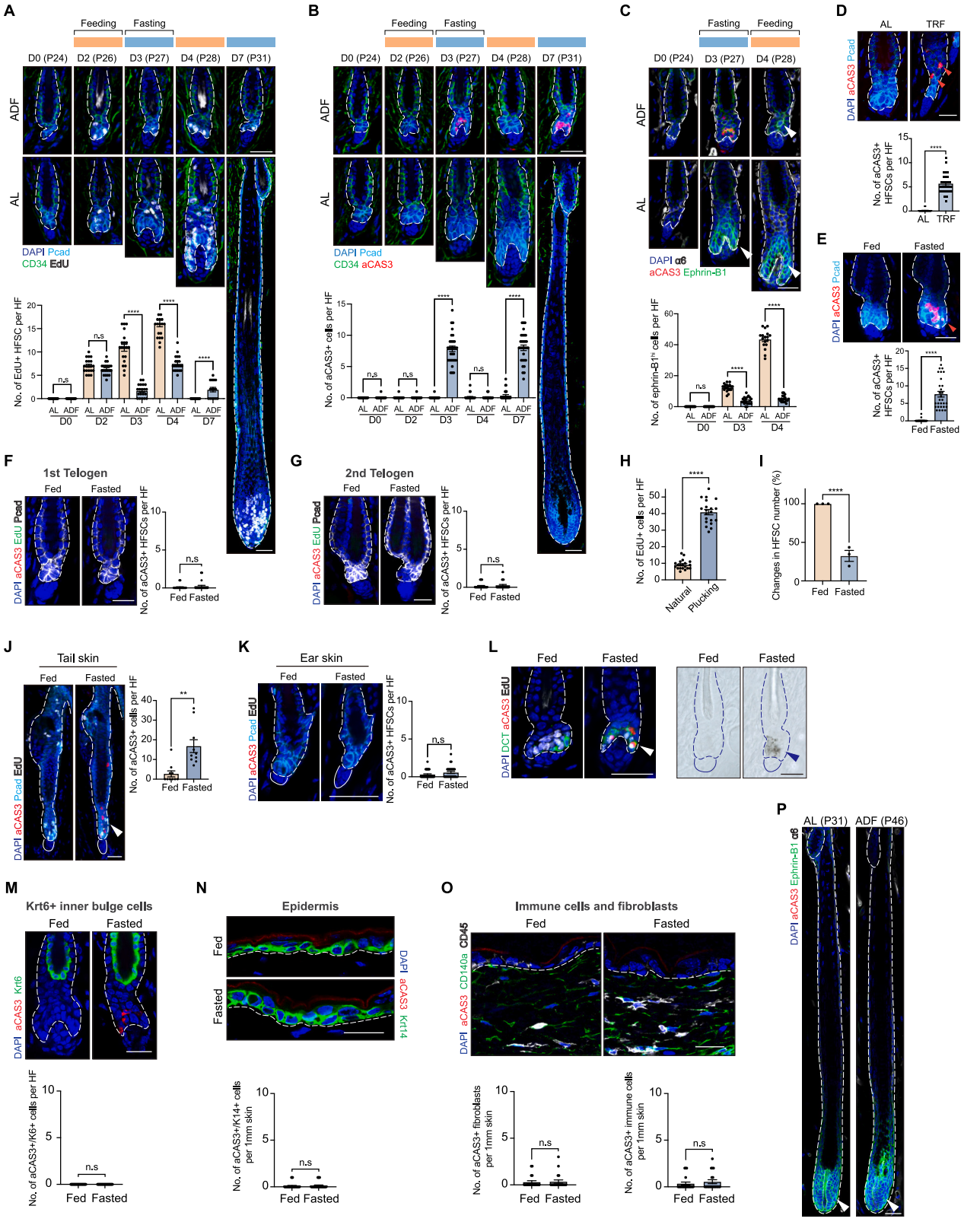

(legend on next page)

Figure S2. HFSC dynamics and the fate of other skin cells under fasting, related to Figure 2

(A) Activation of HFSCs in mice subjected to AL and ADF starting from P24, as shown by immunofluorescent staining for CD34, Pcad, and EdU. Normally the $CD34^{low}/Pcad^{high}$ HFSCs in the hair germ are activated first, followed by $CD34^{high}/Pcad^{low}$ HFSCs in the bulge.

(B) Apoptosis of HFSCs in mice subjected to AL and ADF starting from P24, as shown by immunofluorescent staining for CD34, Pcad, and aCAS3. Bar graphs quantify the number of EdU+ activated HFSCs per hair follicle in (A) or aCAS3+ apoptotic HFSCs in (B) (n = 20 hair follicles from 3 mice for each time point, two-tailed unpaired t test).

(C) Differentiation of HFSCs shown by immunofluorescent staining for ephrin-B1 (green, labeling for differentiated progenies of HFSCs), α6, and aCAS3 in mice subjected to AL or ADF starting from P24. Bar graphs quantify the number of ephrine-$B1^{hi}$ cells per hair follicle (n = 20 hair follicles from 3 mice for each time point, two-tailed unpaired t test).

(D) Representative immunofluorescent staining of hair follicles for aCAS3 (red) from mice under AL and TRF. Red arrowheads mark the apoptotic HFSCs.

(E) Immunofluorescent staining of hair follicles for aCAS3 from mice subjected to AL or ADF starting from 2^{nd} telogen.

(F and G) (F) Immunofluorescent staining of hair follicles for aCAS3 (red) from fed or fasted mice at 1^{st} telogen and 2^{nd} telogen (G), when the HFSCs remain in the quiescent state (n = 30 hair follicles from 3 mice for each group, two-tailed unpaired t test).

(H) Quantification of EdU+ HFSCs during plucking-induced or natural anagen entry.

(I) The number of HFSCs decreases after 24-h fasting (starts from plucking day 2), shown by flow cytometry analysis using K14-H2BGFP mice (n = 3 independent experiments, two-tailed unpaired t test).

(J) Immunofluorescent staining of early anagen hair follicles in tail skin for aCAS3 (red), Pcad (light blue), and EdU (white) from fed or fasted mice (n = 10 hair follicles from 3 mice for each group, two-tailed unpaired t test).

(K) Immunofluorescent staining of hair follicles in ear skin for aCAS3 (red), Pcad (light blue), and EdU (white) from fed or fasted mice (n = 30 hair follicles from 3 mice for each group, two-tailed unpaired t test).

(L) Left: immunofluorescent staining of hair follicles for dopachrome tautomerase (DCT, green, a marker for melanocyte stem cell), aCAS3 (red), and EdU (white) from fasted and fed mice. White arrowhead marks the EdU+/aCAS3+/DCT+ melanocyte stem cell. Right: melanin deposition in the hair germ of fasted mice viewed under a bright field. Blue arrowhead marks the melanin in hair germ.

(M) Immunofluorescent staining of hair follicles for keratin 6 (K6, green, a marker for inner bulge cells) from fasted and fed mice (n = 3 mice for each group, two-tailed unpaired t test).

(N) Immunofluorescent staining of hair follicles for keratin 14 (K14, green, a marker for epidermal stem cells [EpiSCs]) from fasted and fed mice (n = 3 mice for each group, two-tailed unpaired t test).

(O) Immunofluorescent staining of hair follicles for fibroblast marker CD140a (green) and immune cell marker CD45 (white) from fasted and fed mice (n = 3 mice for each group, two-tailed unpaired t test).

(P) Immunofluorescent staining of late anagen hair follicles for ephrine-B1 (green) from AL (P31) or ADF (P46) mice. Scale bars, 30 μm. Data are presented as mean ± SEM. $^{**}p < 0.01$, $^{****}p < 0.0001$, n.s., not significant.

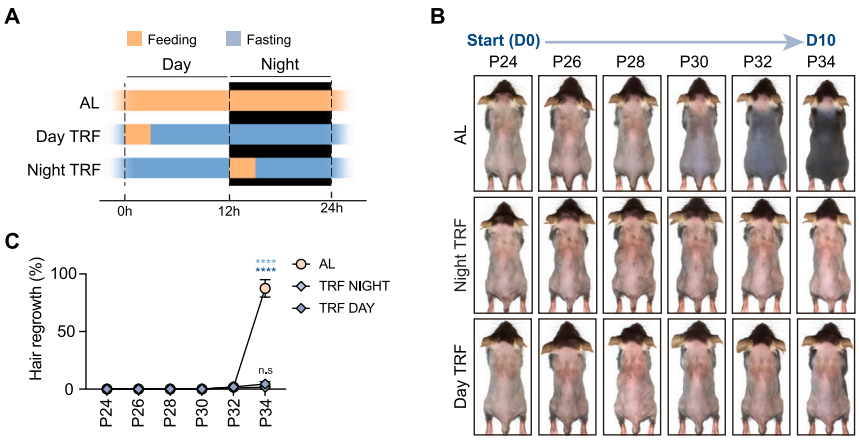

Figure S3. Circadian rhythm changes are not responsible for inhibited hair regeneration, related to Figure 3

(A) Schematic of TRF during the day and during the night.

(B) Progression of hair regrowth in female mice subjected to TRF paradigms during the day or the night between P24 and P34. Mice were shaved before treatments.

(C) Quantification of the hair regrowth in mice in (B) (n = 3–5 mice for each group, two-way analysis of variance [ANOVA] with Dunnett multiple comparisons test). Data are presented as mean ± SEM. ****$p < 0.0001$, n.s., not significant.

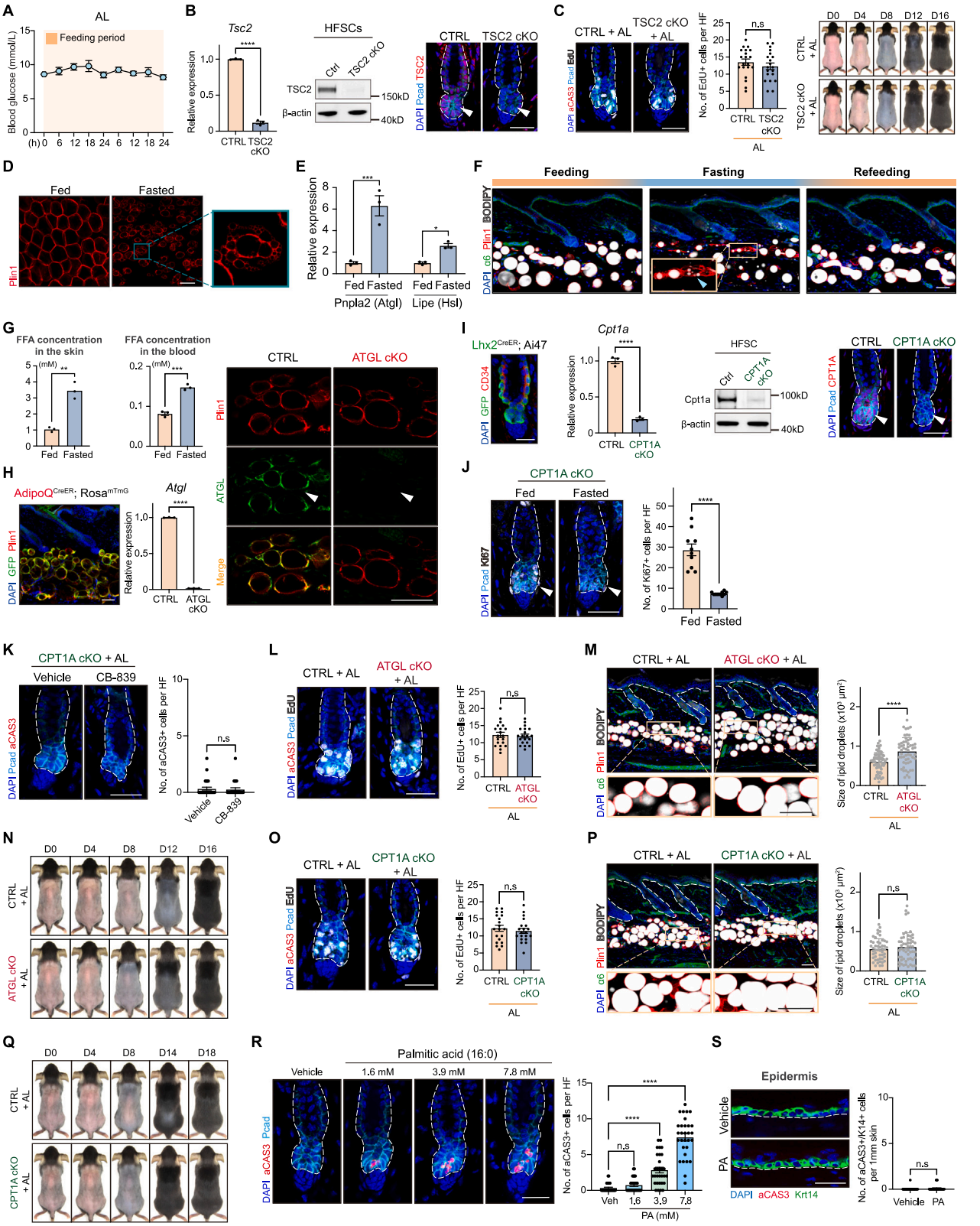

Figure S4. FFAs released through dermal adipocyte lipolysis during fasting induce HFSC apoptosis, related to Figure 4

(legend continued on next page)

(A) Levels of blood glucose change during 48 h in mice under regular AL feeding (n = 6 mice for each time point, one-way ANOVA with Tukey's multiple comparisons test).
(B) Validation of TSC2 knockout efficiency in *K15*^{CreER}*; Tsc2*$^{fl/fl}$ mice through quantitative reverse-transcription PCR (RT-qPCR), western blotting, and immunofluorescent staining.
(C) Left: immunofluorescent staining of hair follicles for EdU and aCAS3 in TSC2 cKO mice under AL and quantification of EdU+ cells per hair follicle (n = 20 hair follicles for each condition, two-tailed unpaired t test). Right: progression of hair regrowth in *K15*^{CrePGR}*; Tsc2*$^{fl/fl}$ mice and littermate controls under AL after hair plucking.
(D) Whole-mount staining of dermal adipocytes for Plin1, a marker outlines the lipid droplets. Green box shows the dermal adipocytes undergoing lipolysis after 24 h of fasting.
(E) RT-qPCR of genes that code key lipolytic enzymes in dermal adipocytes from fed or 24-h fasted mice (n = 3 mice for each group, two-way ANOVA with Dunnett multiple comparisons test).
(F) Dermal adipocytes underwent rapid lipolysis upon fasting and ceased promptly upon refeeding. The blue arrowhead in the immunofluorescence image marks an adipocyte undergoing lipolysis.
(G) Measurement of the free fatty acid (FFA) concentration in the skin (left) and blood (right) after 24-h fasting by ELISA (n = 3 independent experiments for each group, two-tailed unpaired t test).
(H) Testing the labeling of dermal adipocytes using *AdipoQ*^{CreER}*; Rosa*^{mTmG} mice, and validation of ATGL knockout efficiency in *AdipoQ*^{CreER}*; Atgl*$^{fl/fl}$ mice through RT-qPCR and immunofluorescent staining for ATGL (green) and Plin1 (red).
(I) Testing the labeling of HFSCs using *Lhx2*^{CreER}*; Ai47* mice, and validation of CPT1A knockout efficiency in *Lhx2*^{CreER}*; Cpt1a*$^{fl/fl}$ mice through RT-qPCR, western blotting, and immunofluorescent staining for CPT1A (red).
(J) Immunofluorescent staining of hair follicles for Ki67 and Pcad in CPT1A cKO mice under fed or fasted condition and quantification of Ki67+ cells per hair follicle (n = 10 hair follicles for each condition, one-way ANOVA with Tukey's multiple comparisons test).
(K) Immunofluorescent staining for aCAS3 and Pcad in CPT1A cKO mice treated with vehicle or CB-839 under AL conditions (n = 30 hair follicles for each condition, two-tailed unpaired t test).
(L) Immunofluorescent staining of hair follicles for EdU, aCAS3, and Pcad in *AdipoQ*^{CreER}*; Atgl*$^{fl/fl}$ (ATGL cKO) mice and control littermate under AL and quantification of EdU+ cells per hair follicle (n = 20 hair follicles for each condition, two-tailed unpaired t test).
(M) Immunofluorescent staining of dermal adipocytes in ATGL cKO mice under AL and quantification of lipid droplet area (two-tailed unpaired t test).
(N) Progression of hair regrowth in ATGL cKO mice and littermate controls under AL.
(O) Immunofluorescent staining of hair follicles for EdU, aCAS3, and Pcad in *Lhx2*^{CreER}*; Cpt1a*$^{fl/fl}$ (CPT1A cKO) mice and control littermate under AL and quantification of EdU+ cells per hair follicle (n = 20 hair follicles for each condition, two-tailed unpaired t test).
(P) Immunofluorescent staining of dermal adipocytes in CPT1A cKO mice under AL and quantification of lipid droplet area (two-tailed unpaired t test).
(Q) Progression of hair regrowth in CPT1A cKO mice and littermate controls under AL.
(R) Immunofluorescent staining of hair follicles for aCAS3 and Pcad in mice intradermally injected with different concentrations of palmitic acid under AL (n = 30 hair follicles from 3 mice for each condition, one-way ANOVA with Tukey's multiple comparisons test).
(S) Immunofluorescent staining of skin epidermis for K14 after intradermal injection of vehicle or 7.8 mM palmitic acid under AL. Scale bars, 30 μm for (B), (C), (I)–(L), (O), (R), and (S), 50 μm for (D), (F), (H), (M), and (P). Data are presented as mean ± SEM. $^{*}p < 0.05$, $^{**}p < 0.01$, $^{***}p < 0.001$, $^{****}p < 0.0001$, n.s., not significant.

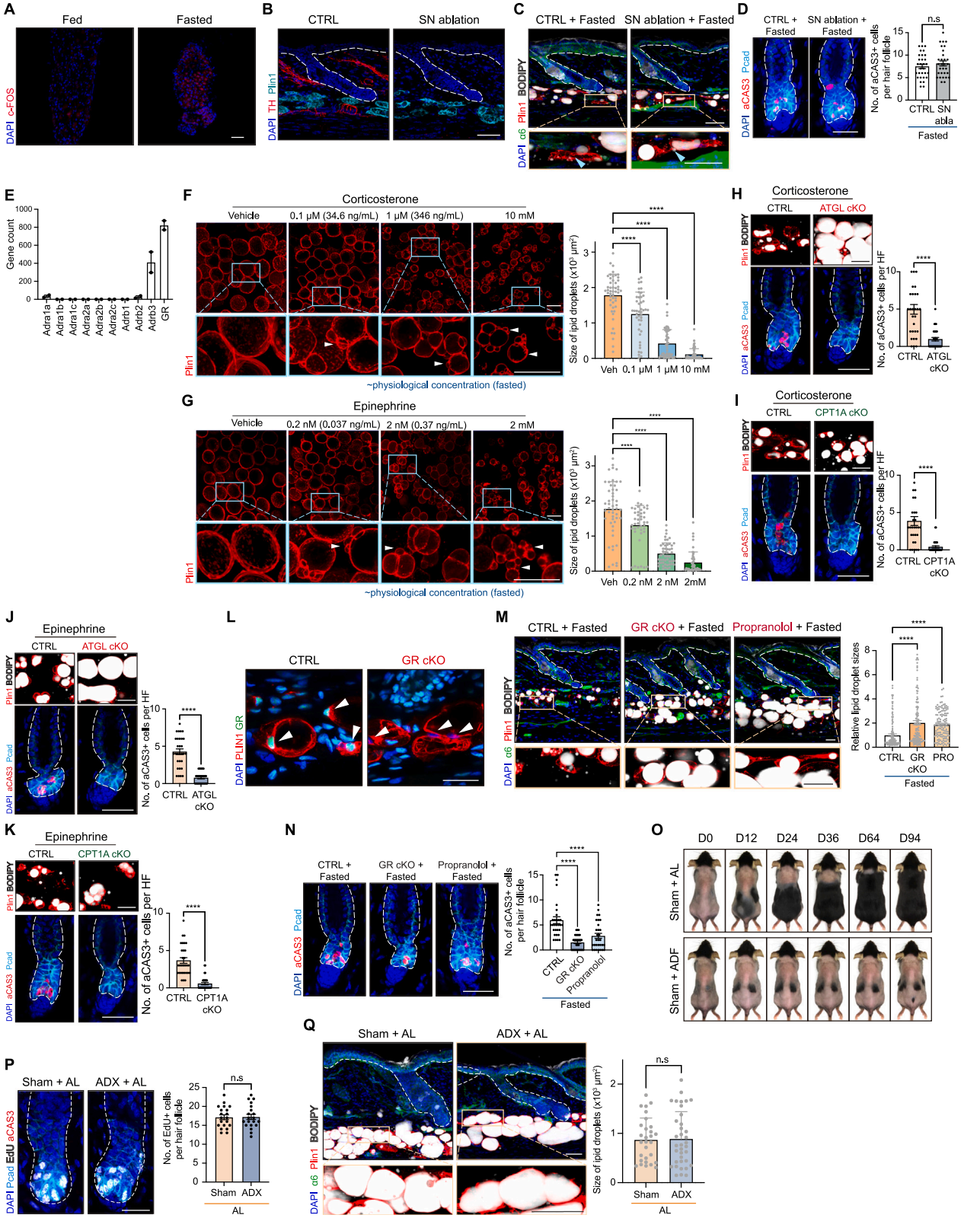

(legend on next page)

Figure S5. Epinephrine and corticosterone released by adrenal glands drive dermal adipocyte lipolysis, related to Figure 5

(A) Immunofluorescent staining of sympathetic ganglia for FOS (red) from fed and fasted mice.

(B) Ablation of sympathetic nerves using 6-hydroxydopamine shown by tyrosine hydroxylase (TH) staining. SN, sympathetic nerve.

(C) Dermal adipocytes still underwent lipolysis in the absence of sympathetic innervation upon fasting.

(D) HFSCs still underwent apoptosis in the absence of sympathetic innervation upon fasting. SN abla, sympathetic nerve ablation.

(E) Gene counts of the adrenergic receptors and glucocorticoid receptors in dermal adipocytes sequencing (n = 2 biologically independent samples from published data).

(F and G) (F) Whole-mount staining of mouse skin explant cultured with the indicated concentration of corticosterone (F) or epinephrine (G) for Plin1. The lipid droplet area was quantified (one-way ANOVA with Tukey's multiple comparisons test).

(H and I) Dermal adipocyte and HFSC apoptosis staining at sites of corticosterone intradermal injection in *AdipoQ^{CreER}; Atgl$^{fl/fl}$* (ATGL cKO) and *Lhx2^{CreER}; Cpt1a$^{fl/fl}$* (CPT1A cKO) mice under AL conditions.

(J and K) Dermal adipocyte and HFSC apoptosis staining at sites of epinephrine intradermal injection in ATGL cKO and CPT1A cKO mice under AL conditions.

(L) Validation of GR knockout efficiency in *AdipoQ^{CreER}; GR$^{fl/fl}$* (GR cKO) mice through immunofluorescent staining for GR (green) and PLIN1 (red).

(M) Reduced fasting-induced lipolysis in dermal adipocytes in GR cKO mice or mice treated with propranolol.

(N) Reduced fasting-induced apoptosis in HFSCs in GR cKO mice or mice treated with propranolol.

(O) Hair regrowth of sham mice under ADF (n = 4–6 mice for each condition).

(P) Immunofluorescent staining of early anagen hair follicles for EdU and aCAS3 in ADX and sham mice under AL and quantification of EdU+ cells per hair follicle (n = 20 hair follicles for each condition, two-tailed unpaired t test).

(Q) Dermal adipocyte staining on ADX or sham mice under AL and quantification of lipid droplet area (two-tailed unpaired t test). Scale bars, 30 μm for (D), (H), (I)–(L), (N), and (P), 50 μm for (A)–(C), (F), (G), (M), and (Q). Data are presented as mean ± SEM. $^{****}p < 0.0001$, n.s., not significant.

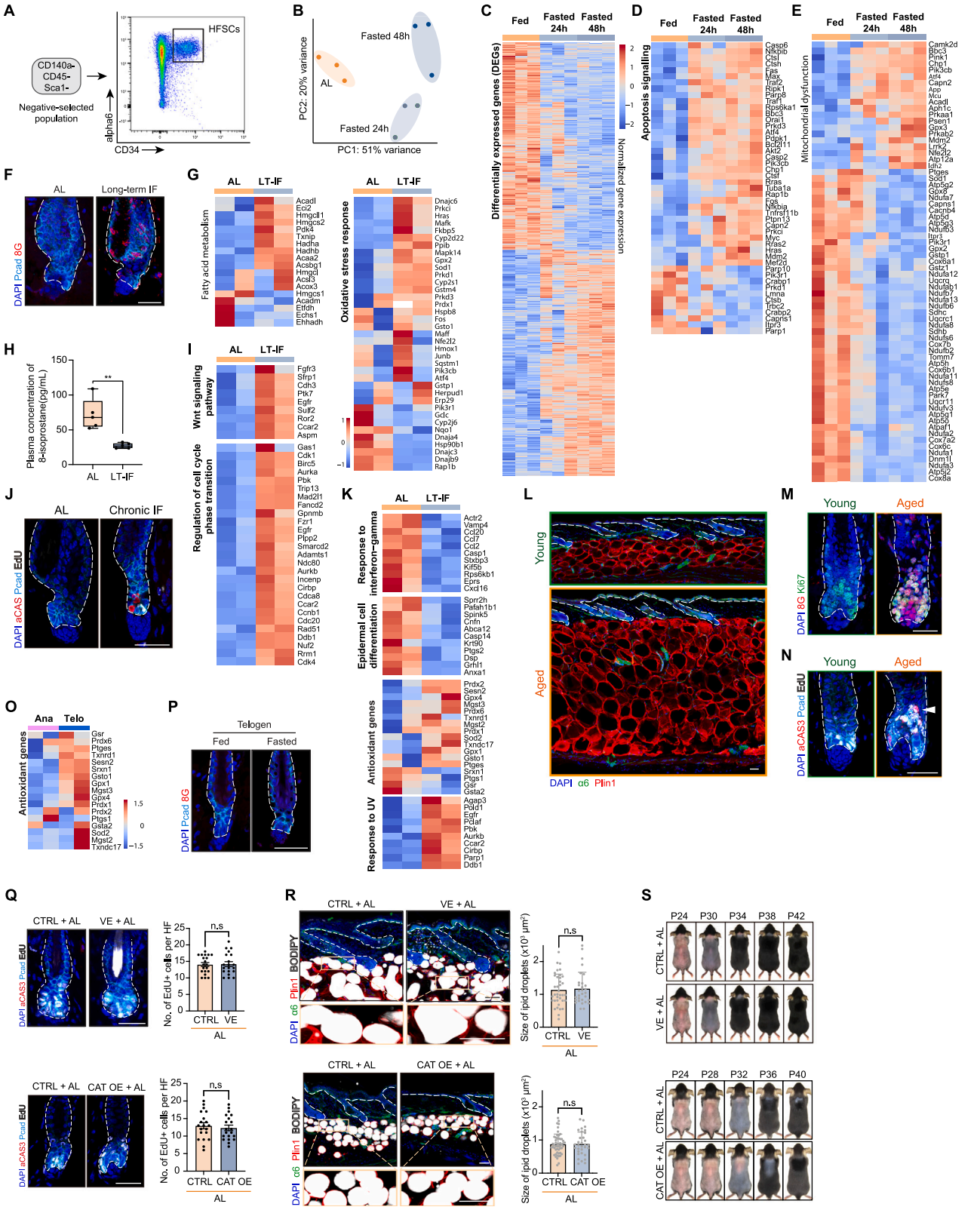

(legend on next page)

Figure S6. RNA-seq analysis of HFSCs from mice under short-term and long-term intermittent fasting, related to Figure 6

(A) FACS strategy for purifying HFSCs: CD140a−, CD45−, Sca1−, CD34+, and alpha6 high cells are sorted as HFSCs.

(B) Principal-component analysis (PCA) of gene expression variation of the three groups.

(C) Heatmap of all differentially expressed genes (DEGs, $n = 3$ biologically independent samples for each condition).

(D and E) (D) Heatmap showing differential expression of signature genes related to apoptosis signaling and (E), mitochondrial dysfunction.

(F) Hair follicles stained with 8G (red) and Pcad (light blue) from AL or long-term intermittent fasting mouse skin.

(G) Heatmap showing differential gene expression related to fatty acid metabolism (left) and oxidative stress response (right) in AL and long-term intermittent fasting (LT-IF) mice HFSCs.

(H) Plasma level of 8-isoprostane in mice subjected to AL and long-term intermittent fasting measured by ELISA.

(I) Heatmap showing differential gene expression related to Wnt signaling pathway and cell cycle phase transition regulation in AL and LT-IF mice.

(J) Immunofluorescent staining of hair follicles for EdU and aCAS3 in mice under 8 months of chronic intermittent fasting.

(K) Heatmap showing differential gene expression related to response to interferon-gamma, epidermal cell differentiation, antioxidant gene expression, and response to UV in AL and LT-IF mice.

(L) Representative dermal adipocyte staining from young (2 months) or aged (24 months) mice.

(M) Representative 8G (red) and ki67 (green) staining of hair follicles from young or aged mice.

(N) Representative HFSC activation (EdU, white) and apoptosis (aCAS3, red) staining in hair follicles from young or aged mice. White arrowhead marks the EdU+ aCAS3+ HFSC in the old mice hair follicle.

(O) Heatmap showing differential expression of antioxidant genes in HFSCs in the early anagen or telogen stage. Ana, anagen; Telo, telogen.

(P) Immunofluorescent staining of telogen hair follicles for 8G (red) in fed or fasted mice.

(Q) Immunofluorescent staining of hair follicles for EdU and aCAS3 in VE-treated mice (top) or catalase overexpression (CAT OE) mice (bottom) under AL and quantification of EdU+ cells per hair follicle ($n = 20$ hair follicles for each condition, two-tailed unpaired t test).

(R) Immunofluorescent staining of dermal adipocytes in VE-treated mice (top) or CAT OE mice (bottom) under AL and quantification of lipid droplet area.

(S) Progression of hair regrowth in VE-treated mice (left) or CAT OE mice and littermate controls under AL (representative images from 3 mice for each group).

Scale bars, 30 μm for (F), (J), (P), (M), (N), and (Q), and 50 μm for (L) and (R). Data are presented as mean ± SEM. $^{**}p < 0.01$, n.s., not significant.

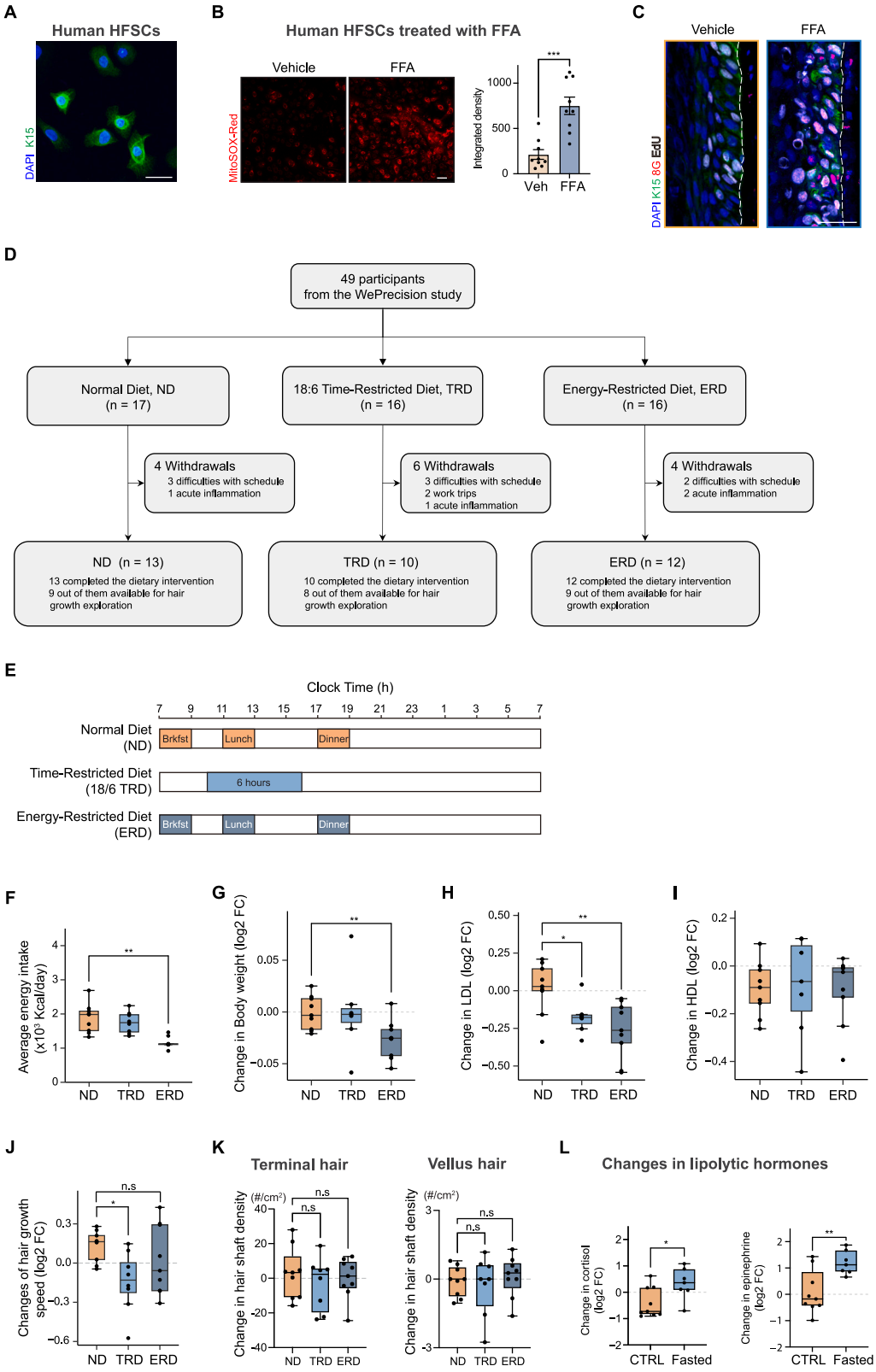

(legend on next page)

Figure S7. Human RCT study design and metabolic health assessment, related to Figure 7

(A) Immunofluorescent staining for K15 (green) in freshly isolated HFSCs from human hair follicles.

(B) MitoSox red staining of cultured human HFSCs treated with palmitic acid and quantification of integrated density using ImageJ.

(C) Representative 8G (red) and EdU (white) staining of human hair follicles treated with palmitic acid or vehicle.

(D) CONSORT diagram showing participant flow through the trial. 49 participants who met the inclusion criteria from the WePrecision-1 study were recruited and randomized into 1 of the 3 groups: normal diet (ND), 18:6 time-restricted diet (TRD), and energy-restricted diet (ERD). After intervention, there were 9 completers in the ND group, 8 completers in the 18/6 TRD group, and 9 completers in the ERD group that were available for hair growth analysis.

(E) Schematic of food available time in WePrecision-2 human trial. Participants in the ND group have access to food at any time. Participants in the 18/6 TRD group can only have meals from 10:00 to 16:00 and fast for 18 h every day. For participants in the ERD group, the daily energy intake was limited to 1,200∼1,500 kcal. The rough range of mealtime was 7:00–9:00, 11:00–13:00, and 17:00–19:00.

(F) Average daily energy intake (kcal) of each group.

(G–I) (G) Boxplots show the $\log_2$ fold change in body weight, serum low-density lipoprotein (LDL) (H), and high-density lipoprotein (HDL) (I) after the intervention.

(J) Hair growth speed alteration ($\log_2$ fold change compared with baseline) after intervention under each condition.

(K) Boxplots illustrate the changes in hair shaft density of terminal and vellus hairs.

(L) Boxplots illustrate the changes in serum cortisol and epinephrine levels in individuals from the ND and TRD groups after 18 h of fasting during the intervention period, compared with their baseline levels. Hormone concentrations were measured using ELISA. Scale bars, 30 μm for (A) and (C), 50 μm for (B). In the bar graph, data are presented as mean ± SEM. In the box plot, data are presented as the interquartile range and median. $^{*}p < 0.05$, $^{**}p < 0.01$, $^{***}p < 0.001$, n.s., not significant.